# Molecular characterization of Rft1, a membrane protein associated with congenital disorder of glycosylation type 1N

Eri Hirata[1‡], Ken-taro Sakata[1‡], Grace I. Dearden[1], Indu Menon[1], George N. Chiduza[2], Anant K. Menon[1]*

[1]Department of Biochemistry, Weill Cornell Medical College, New York, NY 10065, USA
[2]Structure and Function of Biological Membranes - Chemistry Department, Université Libre de Bruxelles - Campus Plaine, 1050 Brussels, Belgium

[‡]Equal contribution
*Correspondence
Anant K. Menon: akm2003@med.cornell.edu

Running title: Molecular characterization of Rft1

Keywords: CDG, dolichol-linked oligosaccharide, endoplasmic reticulum, lipid droplet, MurJ, *N*-glycosylation, scramblase, yeast

## ABSTRACT

The oligosaccharide needed for protein *N*-glycosylation is assembled on a lipid carrier via a multi-step pathway. Synthesis is initiated on the cytoplasmic face of the endoplasmic reticulum (ER) and completed on the luminal side after transbilayer translocation of a heptasaccharide lipid intermediate. More than 30 Congenital Disorders of Glycosylation (CDGs) are associated with this pathway, including CDG 1N which results from defects in the membrane protein Rft1. Rft1 is essential for the viability of yeast and mammalian cells and was proposed as the transporter needed to flip the heptasaccharide lipid intermediate across the ER membrane. However, other studies indicated that Rft1 is not required for heptasaccharide lipid flipping in microsomes or unilamellar vesicles reconstituted with ER membrane proteins, nor is it required for the viability of at least one eukaryote. It is therefore not known what role Rft1 plays in *N*-glycosylation. Here, we present a molecular characterization of human Rft1, using yeast cells as a reporter system. We show that it is a multi-spanning membrane protein located in the ER, with its N and C-termini facing the cytoplasm. It is not *N*-glycosylated. The majority of CDG 1N mutations map to highly conserved regions of the protein. We identify key residues that are important for Rft1's ability to support glycosylation and cell viability. Our results provide a necessary platform for future work on this enigmatic protein.

## INTRODUCTION

Asparagine-linked (*N*-linked) protein glycosylation is found in all three domains of life. In eukaryotes, it occurs in the lumen of the endoplasmic reticulum (ER) where the enzyme oligosaccharyltransferase (OST) attaches a pre-synthesized oligosaccharide (Glucose$_3$Mannose$_9$*N*-acetylglucosamine$_2$ (abbreviated Glc$_3$Man$_9$GlcNAc$_2$, or simply G3M9) in yeast and humans) to asparagine residues within glycosylation sequons in newly translocated proteins (Fig. 1A) (1, 2). The oligosaccharide is assembled by sequentially glycosylating the isoprenoid lipid carrier dolichyl phosphate. This occurs in two stages — the lipid intermediate Man$_5$GlcNAc$_2$-PP-dolichol (M5-DLO) is first generated on the cytoplasmic face of the ER, then elaborated to the mature glycolipid G3M9-DLO after being flipped across the membrane to the luminal side (Fig. 1A) (3-7). The molecular identities of the necessary glycosyltransferases are known, and several of these enzymes have been structurally characterized (1). However, the identity of the protein that flips M5-DLO across the ER membrane is controversial — biochemical studies indicate that it is a scramblase-type lipid transporter capable of equilibrating M5-DLO across the membrane, in an ATP-independent manner and with high specificity (3-6). Defects in *N*-glycosylation underlie numerous human genetic disorders including a heterogeneous group of autosomal-recessive, metabolic diseases termed Congenital Disorders of Glycosylation (CDGs) (8-13). More than 30 CDGs are associated with the core reactions needed to synthesize *N*-glycoproteins in the ER.

CDG type 1N is associated with defects in the membrane protein Rft1 (14-16), which was proposed as the M5-DLO scramblase based on genetic studies in yeast (17-19). Rft1 is essential for the viability of yeast and mammalian cells, and its deficiency results in the accumulation of M5-DLO, depletion of G3M9-DLO and hypoglycosylation of *N*-glycoproteins. This happens even though the enzymes that convert M5-DLO to G3M9-DLO are intact and OST is unaffected. Importantly, although OST can use M5-DLO as a glycan donor, this does not appear to occur in Rft1-depleted cells. One explanation of these data is that in the absence of the purported Rft1 scramblase, M5-DLO accumulates on the cytoplasmic face of the ER where it cannot be used for G3M9-DLO synthesis and/or the OST reaction.

In contrast to these suggestive results pointing to a role for Rft1 in scrambling M5-DLO in cells, biochemical studies indicated that Rft1 is not necessary for scrambling *in vitro*. Thus, we recapitulated M5-DLO scrambling in large unilamellar vesicles reconstituted with a "Triton Extract (TE)", a mixture of all ER membrane proteins extracted with detergent from yeast or rat liver microsomes (5, 6, 20, 21). We found that scrambling in this system is very specific, with higher order glycolipids (Glc$_{1\text{-}2}$Man$_{6\text{-}9}$GlcNAc$_2$-PP-dolichol) and a structural isomer of M5-DLO being scrambled at least an order of magnitude more slowly than M5-DLO (5, 6). Quantitative elimination of Rft1 from TE by affinity chromatography prior to reconstitution did not impact scrambling, indicating that Rft1 is dispensable for activity. In other experiments, we resolved TE proteins by different methods including dye-resin chromatography and velocity gradient sedimentation. When fractions from these separations were reconstituted into liposomes on an equivalents' basis and assayed, M5-DLO scramblase activity could be clearly resolved from Rft1 (5, 21). These results indicate that even if Rft1 has scramblase activity, it's contribution to the overall M5-DLO scramblase activity of the TE is minor.

In a different study, microsomes were prepared from yeast cells in which Rft1 levels had been lowered by using a regulatable promoter to drive down protein expression (22). Analysis of the

cells showed the expected phenotype of Rft1 deficiency, i.e., accumulation of M5-DLO and hypoglycosylation of the reporter glycoprotein carboxypeptidase Y (CPY). However, intact microsomes derived from these cells were able to execute the entire DLO biosynthetic sequence, converting newly synthesized $GlcNAc_2$-PP-dolichol to $Man_9GlcNAc_2$-PP-dolichol, implying that they could scramble M5-DLO. This was confirmed by direct measurement of scrambling using the M5-DLO analog $GlcNAc_2$-PP-$dolichol_{15}$. These results suggest that the inability of Rft1-deficient cells to use M5-DLO is not due to the absence of a scramblase but because some feature of ER architecture in intact cells poses a barrier that is lost when the cells are disrupted.

A role for Rft1 in scrambling M5-DLO was also questioned in a study of the protein in the early diverging eukaryote *Trypanosoma brucei* (23). Rft1-null procyclic (insect-stage) trypanosomes were found to grow normally. They had normal steady state levels of mature DLO and significant *N*-glycosylation consistent with sufficient M5-DLO scramblase activity yet accumulated M5-DLO to a steady state level 30-100-fold greater than found in wild-type cells.

The cumulative data presented above pose a conundrum in that Rft1 is not required for M5-DLO scramblase activity *in vitro* (reconstituted vesicles and microsomes) or in *T. brucei* cells, but clearly plays a role in the metabolic fate of M5-DLO and is essential for the viability of yeast and human cells. Thus, it remains to be determined what role Rft1 might play in *N*-glycosylation and how its deficiency results in CDG 1N. As a first step towards resolving these issues, we chose to characterize the protein. Rft1 is relatively under-studied, with no published reports concerning its sub-cellular localization, membrane topology and structure-function aspects in yeast and human cells. Here, we present a molecular characterization of human Rft1 (hRft1), using the yeast *Saccharomyces cerevisiae*, a good model system for the study of CDGs (24). We show that the protein is localized throughout the ER and has a polytopic arrangement with its N and C-termini facing the cytoplasm. The majority of CDG 1N mutations map to highly conserved regions of the protein. Using a suite of assays to correlate protein expression, CPY *N*-glycosylation and cell doubling time, we identify key residues that are important for Rft1's ability to support glycosylation and cell viability. These results provide a necessary platform for future work on Rft1.

## RESULTS AND DISCUSSION

### Functional replacement of yeast Rft1 by human Rft1

We used standard yeast genetics methods to generate the haploid strain KSY512 (Table 2) from a heterozygotic diploid strain (*rft1::KANMX4 / RFT1*) which we obtained from the Yeast Knockout Collection (25). We transformed the diploid cells with a *URA3* plasmid (p416-$P_{GPD}$-hRFT1-3xFLAG) (Table 1) encoding human Rft1 (hRft1) with a C-terminal 3xFLAG tag. The transformed cells were sporulated, and individual spores lacking endogenous *RFT1* but carrying the hRft1-expressing *URA3* plasmid were selected on the basis of G418 resistance and ability to grow on plates lacking uracil. We chose cells with mating type 'a' for subsequent experiments.

The KSY512 cells grew on synthetic Ura- media (SD(-Ura)) as expected but did not grow on plates containing 5-fluororotic acid (5-FOA) (Fig. 1B), which is converted by the plasmid-encoded *URA3* gene product into toxic 5-fluorouracil, indicating the essentiality of the p416-$P_{GPD}$-hRFT1-3xFLAG plasmid in these cells. In contrast, isogenic wild-type BY4741 cells did not grow on Ura- media but grew on 5-FOA. These results demonstrate that yeast Rft1 can be functionally replaced by hRft1, as noted previously (14), and that the C-terminal 3xFLAG tag does not appear to affect

hRft1 function, consistent with a previous report in which functional yeast Rft1 was expressed with a C-terminal Protein A tag (20). We used quantitative immunoblotting against the 3xFLAG epitope to assess the hRft1 expression level and found it to be about 800 copies per cell (Fig. S1A, B), which is unexpectedly low given that we used the strong, constitutively active GPD promoter (26) to drive expression. Of note, the reported copy number for endogenous yeast Rft1 is ~1000 molecules/cell (27).

To verify that hRft1 expression supports normal *N*-glycosylation, we analyzed the steady-state *N*-glycosylation status of CPY, a vacuolar protein in yeast with four *N*-glycans (28). Cell samples were processed for SDS-PAGE followed by immunoblotting with anti-CPY antibodies, and the resulting pattern of CPY glycoforms was quantified to obtain a glycosylation score (29)(Fig. 1C). The CPY profile in both wild-type and KSY512 cells was dominated by a single band corresponding to fully *N*-glycosylated mature CPY, although there appeared to be some hypoglycosylation in KSY512 cells as evinced by a faint ladder of lower molecular weight bands corresponding to CPY with <4 *N*-glycans (Fig. 1C). The corresponding glycosylation scores were ~90 (wild type) versus ~75 (KSY512). We conclude that hRft1 can functionally replace yeast Rft1.

## Rft1 localizes to the ER

We next examined the sub-cellular localization of hRft1. For this, we generated a fluorescently tagged hRft1 construct, with mNeonGreen (mNG) (30), a monomeric green/yellow fluorescent protein, fused to its N-terminus. The construct — referred to as mNG-hRft1 — also contains an ALFA-tag (31), N-terminal to mNG, and a C-terminal 3xFLAG tag.

We used plasmid shuffling to test whether mNG-hRft1 is functional. Thus, we transformed KSY512 cells with a *HIS3* plasmid encoding mNG-hRft1 under control of the GPD promoter, then tested the cells for growth on 5-FOA plates. Fig. 1D (right panel, row 3) shows that mNG-hRft1 is functional as the cells grow on the 5-FOA plate. Of note, mNG-hRft1-expressing cells grew better than those expressing hRft1 (Fig. 1D, right panel, compare rows 2 and 3), which may be due to the considerably higher level of expression of mNG-hRft1 (Fig. S1C), possibly the result of a stabilizing effect of the N-terminal tag.

To investigate its sub-cellular localization by fluorescence microscopy we next integrated mNG-hRft1 in the genome of wild-type cells expressing the luminal ER marker mCherry-HDEL. Figure 1E shows that mNG-hRft1 displays a characteristic yeast ER pattern, mainly comprising cortical and nuclear ER regions and overlapping precisely with the distribution of mCherry-HDEL. As this pattern was also observed for mNG-hRft1 constructs expressed under the control of constitutive promoters of different strengths (GPD>TEF>ADH) (Fig. S2) (26) it is not the result of mis-localization due to saturation of trafficking mechanisms. Thus, we demonstrate that hRft1 is an ER-localized protein, consistent with a role in core *N*-glycosylation.

## Is Rft1 localized to an ER domain?

We previously proposed that early steps of DLO synthesis may be laterally segregated from the M5-DLO scramblase in the ER (5), and that a possible role of Rft1 may be to chaperone M5-DLO within the plane of the membrane, from its site of synthesis to the scramblase. This would account for why Rft1 is important in cells where DLO synthesis is laterally compartmentalized, but not in reconstituted systems or in microsomes where compartmentalization might be lost. A related

scenario was proposed for Lec35/MPDU1, another protein with an enigmatic role in *N*-glycosylation (32, 33).

Consistent with our idea, Krahmer et al. (34) reported that several enzymes needed to convert dolichyl-P to M5-DLO on the cytoplasmic face of the ER (Fig. 1A) — including Alg14, the membrane-bound subunit of the heterodimeric GlcNAc transferase complex (35-37), and the mannosyltransferases Alg1, Alg2 and Alg11 — can be co-isolated with lipid droplets (LDs) in insect cells. They also reported that Rft1 was located exclusively in the LD fraction. In contrast, the luminally-oriented glycosyltransferases that convert M5-DLO to G3M9-DLO do not associate with LDs. The hydrophobic portion of Alg14 adopts conformations that enable it to integrate into both membrane bilayers as well as phospholipid monolayers, such as those that surround LDs (38, 39), accounting for its enrichment in the LD proteome. The mechanism by which Alg1, Alg2, Alg11 and Rft1 might associate with LDs is likely different — these membrane proteins may reside in a domain of the ER that wraps around LDs (40) and thus co-isolates with these organelles. These observations suggest that the DLO pathway is not only transversely segregated across the ER membrane as depicted in Figure 1A, but also laterally compartmentalized with M5-DLO being generated in an ER domain that can be isolated and visualized via its association with LDs.

To test this scenario in our yeast model, we transformed wild-type yeast cells expressing the lipid droplet marker Erg6-mCherry (41) with plasmids encoding mNG-tagged Alg14 and Alg2. The cells were grown in rich medium supplemented with oleic acid to induce lipid droplets and examined by fluorescence microscopy. We found that Alg14 co-localized strongly with LDs, visualized as ring-like structures marked by Erg6-mCherry (Fig. 2A), whereas Alg2 displayed a typical ER pattern, distinct from LDs (Fig. 2B). We next integrated mNG-hRft1 in the genome of the Erg6-mCherry-expressing cells and examined its localization after LD induction. We used both GPD and ADH promotors to ensure that the outcome of the experiment did not depend on protein expression level. Figure 2C shows that mNG-hRft1 retains its pan-ER distribution (as in Fig. 1E and Fig. S2) in oleic acid-fed cells distinct from the Erg6-mCherry-marked LD structures. We note, however, the presence of mNG-hRft1-containing ER strands that appear to be closely apposed to LDs (Fig. 2C, arrowheads) — whether these strands represent genuine contact between the two organelles or simply appear as a result of crowding is unclear, but we did not see them in mNG-Alg2-expressing cells (Fig. 2B). These results differ from those of Krahmer et al. (34) (summarized below).

## Consequences of restricting Rft1 to an ER domain

To pursue the idea that lateral segregation of the DLO biosynthetic pathway may nevertheless underlie a possible function of Rft1, we next took a complementary approach in which we tested the consequence of restricting Rft1 to an ER domain. For this we took advantage of a method described by Fröhlich and coworkers (42) in which they used a nanobody-based system to restrict localization of an ER membrane protein to the nuclear ER. Accordingly, we used our mNG-hRft1 construct which has an ALFA-tag at its N-terminus and expressed it in cells in which a nanobody directed against the ALFA-tag is fused to the membrane anchor of Nvj1 to recruit Rft1 to the nuclear ER. We used cells in which expression of endogenous Rft1 is under control of a Tet-off promoter; these cells fail to grow in doxycycline (Dox) (Fig. S3A). Using the ADH promoter for expression, we could quantitatively restrict mNG-hRft1 to the nuclear ER (Fig. S3B; expression from the stronger GPD promoter was not as efficient, presumably because the nanobody capture

system was saturated by highly expressed mNG-hRft1). However, the cells showed no growth phenotype when grown on Dox (Fig. S3C), indicating that restriction of hRft1 to the nuclear ER does not affect its function.

We conclude that at the level of resolution used in these studies, the synthesis of M5-DLO is partly confined to LDs as evinced by co-localization of Alg14 with these organelles. However, the Alg2 mannosyltransferase and Rft1 do not colocalize with LDs as reported previously (Fig. 2C), nor are cells affected when the majority of Rft1 is confined to the nuclear ER (Fig. S3B,C).

## Rft1 is not necessary for M5-DLO scramblase activity in liposomes reconstituted with total ER membrane proteins

We next re-assessed the hypothesis that Rft1 is responsible for scrambling M5-DLO across the ER membrane. We prepared a salt-washed microsomal fraction from a homogenate of KSY512 cells, selectively extracted ER membrane proteins with ice-cold Triton X-100 as previously described (5) and reconstituted the protein mixture (Triton Extract (TE)) into large unilamellar vesicles composed of egg phosphatidylcholine (egg PC), with trace quantities of [$^3$H]M5-DLO and a fluorescent PC analog, NBD-PC, which has a nitrobenzoxadiazole (NBD) fluorophore attached to one of its acyl chains. In parallel, we incubated an identical sample of TE with anti-FLAG resin to remove hRft1-3xFLAG, before reconstituting it into LUVs. Protein-free liposomes were also prepared. Immunoblotting analysis showed that anti-FLAG treatment quantitatively and specifically removed hRft1-3xFLAG from TE — no FLAG signal was detected in the treated sample, whereas the signal corresponding to an irrelevant ER protein, Dpm1, was unchanged (Fig. 3A). Dynamic light scattering indicated that the vesicle samples were similar, with an average diameter of ~175 nm (Fig. 3B).

We previously showed that proteoliposomes reconstituted with yeast TE have glycerophospholipid scramblase activity (5, 43), reflecting the biogenic properties of the ER (3, 4, 44). As this activity is not expected to be related to Rft1, we used it as a control to compare proteoliposomes prepared with anti-FLAG-resin-treated TE versus mock-treated TE. We assayed the activity as previously described by measuring the ability of the membrane-impermeant reductant dithionite to bleach NBD-PC molecules in the outer leaflet of reconstituted vesicles. For protein-free liposomes, NBD-PC molecules in the inner leaflet are protected, whereas for proteoliposomes containing scramblases, these molecules are scrambled to the outer leaflet where they are exposed to dithionite. Thus, approximately half the fluorescence of protein-free liposomes is expected to be lost on dithionite treatment, whereas a larger proportion of fluorescence should be lost in a vesicle population where some or most vesicles contain a functional scramblase. This is indeed what we observed (Fig. 3C) — dithionite treatment of protein-free liposomes resulted in a drop of ~57% of fluorescence, whereas for proteoliposomes, irrespective of whether they were generated from anti-FLAG-resin-treated TE or mock-treated TE, the drop was ~80% (the traces are identical, hence they are shown displaced from one another for easy visualization (Fig. 3C)). These numbers indicate that, at the protein/phospholipid ratio used for reconstitution, approximately 55% of the vesicles contain a phospholipid scramblase (calculated as described (45)). Furthermore, the identical fluorescence reduction traces obtained for proteoliposomes generated from the treated and mock-treated samples indicate that these vesicles are similarly reconstituted.

We next assayed the same vesicles for M5-DLO scramblase activity, using a previously described assay (5, 20, 21) in which the mannose-binding lectin Concanavalin A (Con A) is used to capture M5-DLO molecules located in the outer leaflet of the vesicles. For protein-free vesicles, half the M5-DLO molecules are expected to be captured at the endpoint of the assay as the remainder are confined to the inner leaflet. For proteoliposomes with M5-DLO-scramblase activity, all M5-DLO molecules are expected to be captured as those from the inner leaflet are translocated to the Con A-accessible outer leaflet. As shown in Figure 3D, ~50% of M5-DLO is captured in protein-free liposomes as expected, whereas ~65% is captured in both types of proteoliposomes. Thus, the presence or absence of Rft1 does not affect the outcome of the M5-DLO scramblase assay. We note that a larger proportion of proteoliposomes contain phospholipid scramblase activity compared with M5-DLO scramblase activity, ~55% versus ~30%, respectively (calculated as described (45)), consistent with the greater abundance of phospholipid scramblase(s) in the TE as reported previously (5).

Thus, proteoliposomes generated from an extract of ER membrane proteins, *sans* Rft1, have undiminished M5-DLO scramblase activity compared with Rft1-replete vesicles. This updated result, building on a new yeast test strain expressing hRft1 and additional quality controls for vesicle reconstitution, extends our previous conclusion (20) that Rft1 is not required for scrambling in our reconstitution-based assay. If Rft1 does indeed have M5-DLO scramblase activity, a possibility that can be tested in the future when high-quality purified protein is available, it would appear to be a minor contributor, and redundant with other scramblases as our reconstitution data clearly indicate that the majority of the scramblase activity in the TE is due to another protein(s). A back-of-the-envelope analysis of vesicle occupancy data determined in a previous reconstitution-based study of M5-DLO scramblase activity (5) indicates — with standard assumptions concerning vesicle diameter, cross-sectional area of a phospholipid and the average molecular mass of ER membrane proteins — that the M5-DLO scramblase represents $\geq$ 1% by weight of proteins in the TE. As there are approximately $2 \times 10^6$ ER membrane proteins in a haploid yeast cell (46), we conclude that there are at least 20,000 M5-DLO scramblases. In contrast, there are only <1000 copies of hRft1 per cell in the KSY512 strain used for the present analysis (Fig. S1A, B).

## Architecture of hRft1

Structure prediction by AlphaFold (47, 48) reveals that hRft1 has 14 transmembrane (TM) spans (Fig. 4A,C). Although residues in a portion of TM1, the disordered C terminus, and intracellular loop 3 had predicted Local Distance Difference Test (pLDDT) (47) scores below 70, the remaining residues had higher scores indicating the good quality of the model. The DeepTMHMM topology prediction program (49) also indicates a 14-TM model, additionally placing the N-terminus and C-terminus of the protein on the cytoplasmic side of the membrane. Our data are consistent with this arrangement as we showed that the ALFA-epitope-tagged N-terminus of mNG-hRft1 is oriented to the cytoplasm where it can interact with the anti-ALFA nanobody-Nvj1 fusion construct (Fig. S3B). A prediction of the topology model (Fig. 4A) is that the only *N*-glycosylation sequon in the protein ($N^{227}IT$) is located in intracellular (cytoplasmic) loop 3 where it cannot be glycosylated. To test this, we treated an extract of KSY512 cells with PNGase F. SDS-PAGE immunoblotting revealed that the quadruply glycosylated CPY glycoform collapsed to a lower molecular weight, non-glycosylated band upon treatment (Fig. 4B, right panel), whereas hRft1 (detected via its C-

terminal 3xFLAG tag) was not affected (Fig. 4B, left panel). This result is consistent with the location of N227 in a cytoplasmic loop and with the topology prediction (Fig. 4A). Of note, we previously showed that M5-DLO scramblase activity is associated with ER proteins or protein complexes that bind Con A-Sepharose (50) — this point distinguishes Rft1, which we now show is not a glycoprotein, from the protein (or proteins) that contribute the majority of M5-DLO scramblase activity. This result reinforces our conclusion based on Figure 3D that Rft1 does not contribute to the M5-DLO scramblase activity of the TE in reconstituted vesicles.

Both the AlphaFold model and an HHpred search (51) of the Protein Data Bank indicate that hRft1 has a fold resembling that of members of the multidrug/oligosaccharidyl-lipid/polysaccharide (MOP) family of transporters (52), with structural homology to bacterial MurJ lipid II flippases which are proposed to operate by an alternating access mechanism powered by membrane potential (53-56). The Alphafold model shows hRft1 in an inward-open conformation. The N- and C-terminal lobes define a central hydrophilic region corresponding to a putative substrate binding pocket which is 2.3 nm wide at the membrane-water interface and open to the cytoplasm (Fig. 4C). We used the ConSurf bioinformatics tool (57, 58) to investigate the evolutionary conservation of residues in hRft1 and found high conservation in this hydrophilic region (Fig. 4D). Most of the known CDG1N disease mutations (Table 3) mapped to this region, an interesting exception being the R37 residue (disease variant R37L, Table 3) which is located on the luminal side of the protein where it is potentially involved in stabilizing the interaction between the N- and C-terminal lobes in the modelled conformation (Fig. 4D; Table 3).

Several charged residues (R37, R63, R290, R442, E260) are fully conserved in Rft1 sequences (Fig. 4D, ConSurf scores of 8 or greater), and these are mostly located in the hydrophilic central region. Arginine residues are also found in the central cavity of MurJ where they are required for function (54). The TM1 helix is strongly amphipathic with a conserved Q4-R8-F12-N15 motif, the three hydrophilic residues (Q21, R25, N32) clustering to one side of the helix (Fig. 4A) (52). Using evolutionary coupling analysis (53, 59, 60), we identified A155 as a potentially interesting residue. Although this residue is not highly conserved (ConSurf grade = 6), the PROVEAN protein webserver (61) indicates that a charge substitution, A155E or A155K, would be deleterious to function.

## Functional test of hRft1 variants with point mutations

We next chose to develop a structure-function model of hRft1, using the yeast system to test the functional consequences of introducing mutations at key sites. We chose a number of the sites described above (Fig. 4A) for mutagenesis; we also included two CDG1N mutations for analysis (R25W, which is part of the hydrophilic cluster in TM1, and R67C, which was the first CDG1N mutation to be identified (14)). Using a plasmid shuffling approach we tested the ability of the hRft1 point mutants to support growth. Thus, we transformed KSY512 cells with *HIS3* plasmids encoding hRft1-3xFLAG point mutants under control of the GPD promoter, then tested the cells for growth on 5-FOA plates. Figure 4E shows that of the 10 mutants that we tested, only R25W, R290A, R442A and potentially R63A failed to support growth. To determine whether this was a result of low protein expression, we transformed wild-type cells with the same plasmids and analyzed the expression level of the constructs by immunoblotting. Figure S4 shows that these variants are expressed at reasonable levels compared with most of the other constructs, indicating that their phenotype is directly due to loss of function. Surprisingly, the Q21L and R37A mutants were poorly expressed yet supported growth (Fig. S4).

We verified the overall pattern of functionality seen in the plasmid shuffling experiment by testing the mutant constructs in a yeast strain in which endogenous Rft1 expression is controlled by the Tet-off system (Fig. S3A). Figure 4F shows that cells expressing the R25W, R290A, and R442A variants failed to grow on Dox, and R63A-expressing cells grew poorly, consistent with the data shown in Figure 4E. Cells expressing the other 6 variants grew normally (Fig. 4F).

To obtain more quantitative information, we made use of the KSY512 cells that we recovered from the plasmid shuffling experiment (Fig. 4E); these cells express hRft1 variants that retain some functionality, enabling growth. Quantitative measurements of cell growth over a 36-h period (Fig. 5A) showed that growth was slowed significantly in the three strains expressing R63A, R67A and E260A (Fig. 5B). Immunoblotting analysis (Fig. 5C, D) indicated that all proteins were reasonably expressed in comparison with wild-type protein, except for R37 which was expressed at a very low level as we noted previously (Fig. S4). We carried out additional immunoblotting to assess the steady state glycosylation status of CPY (Fig. 5C, E). Compared with cells expressing the wild-type protein which had a CPY Glycoscore of ~75 (as noted also in Fig. 1B), CPY was hypoglycosylated in all strains expressing the hRft1 mutants, with Glycoscores in the range 50-60 (Fig. 5E).

Closer examination of these data (Fig. 5F-H) revealed several points of interest. Faster growing strains had generally higher CPY Glycoscores, except for the strain expressing E260A which grew slowly despite reasonable glycosylation (Fig. 5F). The R37A variant appeared to be hyperactive (Fig. 5G, H): it was poorly expressed (Fig. S4 and Fig. 5D) yet enabled normal cell growth (Fig. 5B) and supported an average level of CPY glycosylation (Glycoscore ~60) (Fig. 5E). Because R37 may stabilize the interaction between the N- and C-terminal lobes in the inward-open conformation of hRft1 (see above)(Fig. 4C), a mutation at this site may result in reduced stability, favoring conformational switching. R63A had the poorest CPY Glycoscore of the mutants that we tested, despite a normal expression level, and the disease mutant R67C seemed to be functionally compromised — it was the most highly expressed of all the variants we tested, including the wild-type protein, yet cells expressing this variant underperformed in terms of CPY Glycoscore and doubling time (Fig. 5G, H). To determine if the mutant proteins were correctly localized to the ER, we integrated N-terminal mNG-tagged variants of R37A, R63A, R67C and E260A into yeast cells. Fluorescence microscopy revealed a typical ER pattern for all constructs, except for the presence of occasional varicosities in the cortical ER, seen in over half the R63A and R67C-expressing cells (Fig. S5).

## Concluding remarks

Rft1 is nearly ubiquitously found in eukaryotes (62) where it plays a critical yet undefined role in protein *N*-glycosylation. Despite its importance, a basic molecular characterization of the protein is not available, and this is what we have provided in this paper. We show that hRft1 is a polytopic ER membrane protein (Figs. 1E, 2C, 4A), with its N- and C-termini oriented to the cytoplasm (Fig. 4A). It is not *N*-glycosylated (Fig. 4B). The AlphaFold model of hRft1 (Fig. 4C) resembles that of the inward-open conformation of an alternating access transporter, with a hydrophilic cavity open to the cytoplasm (Fig. 4D). The cavity contains several charged residues that are conserved in all Rft1 sequences and which we demonstrate to be functionally important by quantifying the ability of the corresponding point mutants to support cell growth and *N*-glycosylation in a yeast model system (Fig. 4E,F, Fig. 5).

Rft1 belongs to the MOP superfamily of transporters (52) which includes the bacterial MurJ flippases which export Lipid II, a cytoplasmically synthesized undecaprenyl diphosphate-linked peptidoglycan building block, across the membrane to the periplasmic side (3, 63). MurJ proteins are proposed to operate by an alternating access mechanism in which transbilayer export of Lipid II is coupled to the movement of a counterion down its electrochemical gradient (56). The structural similarity between hRft1 and bacterial MurJ flippases (Fig. 4C), and between M5-DLO and Lipid II (3), revives the possibility that Rft1 may play a role in translocating M5-DLO across the ER membrane for *N*-glycosylation. However, many issues and questions need to be considered.

First, in contrast to MurJ-catalyzed lipid export which requires membrane potential (56), transbilayer translocation of M5-DLO and other isoprenoid-based lipids in the ER appears to be mediated by scramblases which equilibrate lipids between the two leaflets of the bilayer independent of metabolic energy inputs (5, 50, 64). Second, as noted in the Introduction, data from cell-free systems indicate that Rft1 is not necessary for M5-DLO scrambling and that scrambling is primarily accomplished by another protein or protein complex in the ER (5, 20-22). Thus, as we show here, the M5-DLO scramblase activity of proteoliposomes reconstituted with ER membrane proteins is unaffected by Rft1 (Fig. 3D); furthermore, Rft1 is not glycosylated (Fig. 4B) whereas M5-DLO scramblase activity is associated with ER glycoproteins or glycoprotein complexes (50). This result does not rule out a transport function for Rft1 — something that can be tested in the future by assaying purified protein in a reconstituted system — but leaves open the question of the precise nature of the lipid or other substrate being transported and whether this transport function underlies Rft1's essentiality in yeast and mammalian cells. A detailed investigation of these points awaits future work.

## EXPERIMENTAL PROCEDURES

### Plasmids

The plasmids used in this paper are listed in Table 1. Plasmids were propagated using DH5-α *E. coli* cells which were cultured at 37°C and 210 rpm in LB+Amp medium (1% tryptone, 0.5% yeast extract, 1% NaCl, and 100 µg/ml ampicillin). Plasmid construction was as follows:

EcAKM135 (p413-$P_{GPD}$-hRFT1-3xFLAG) and EcAKM141 (p413-$P_{GPD}$-hRFT1$^{R67C}$-3xFLAG): hRFT1-3xFLAG and hRFT1$^{R67C}$-3xFLAG fragments were PCR amplified from plasmids AP63 and AP65, respectively, and inserted into BamHI-HindIII-digested p413-$P_{GPD}$ vector using the NEBuilder HiFi DNA Assembly kit (New England Biolabs, E5520S).

EcAKM147 (p413-$P_{GPD}$-ALFA-mNG-hRFT1-3xFLAG): the mNeonGreen fragment was amplified from pFA6a-2xmNeonGreen-kanMX and inserted into EcAKM135 using the NEBuilder HiFi DNA Assembly kit. Next, the ALFA-tag was inserted between $P_{GPD}$ and mNeonGreen by PCR-based site-directed mutagenesis.

EcAKM148 (p413-$P_{TEF}$-ALFA-mNG-hRFT1-3xFLAG): the GPD promoter in EcAKM136 was replaced with the TEF promoter from p413-$P_{TEF}$ by traditional cloning methods using XbaI and XhoI to generate the necessary fragments. The ALFA-tag was inserted as above.

EcAKM149 (p413-$P_{ADH}$-ALFA-mNG-hRFT1-3xFLAG): the $P_{GPD}$ promotor of EcAKM147 was replaced with the $P_{ADH}$ fragment digested from p415-$P_{ADH}$ with SacI and XbaI.

EcAKM150-152 (pCfB2195-$P_{GPD/TEF/ADH}$-ALFA-mNG-hRFT1-3xFLAG): $P_{GPD/TEF/ADH}$-ALFA-mNeonGreen-hRft1-3xFLAG fragments were PCR amplified from EcAKM147-149 and cloned into pCfB2195 digested with AsiSI using the NEBuilder HiFi DNA Assembly kit.

EcAKM153 (pRG205MX-mCherry-HDEL) and EcAKM154 (pRG205MX-$P_{ADH}$-Nvj1$^{1-121}$-ALFA-nB): mCherry-HDEL and $P_{ADH}$-Nvj1$^{1-121}$-ALFA-nB were inserted into pRG205MX. Insertion and vector fragments were created by digesting pRS305-mCherry-HDEL (pJF132), pRS405-$P_{ADH}$-Nvj1$^{1-121}$-ALFA-nB (FFP386), and pRG205MX, respectively, with SacI and XhoI. The AscI site in the ADH terminator region of EcAKM153 was mutated by PCR-based site-directed mutagenesis.

EcAKM162 (p416-mNG-Alg2) and EcAKM163 (p416-mNG-Alg14): the hRft1-3xFLAG sequence of EcAKM170 was replaced with Alg2 or Alg14 fragments amplified from pGB1805-Alg2 and pGB1805-Alg14, respectively.

*RFT1* mutants were created by PCR-based site-directed mutagenesis using p413-$P_{GPD}$-hRFT1-3xFLAG (EcAKM135) or pCfB2195-$P_{GPD}$-ALFA-mNG-hRFT1-3xFLAG (EcAKM150) as templates.

## Yeast strains and culture conditions

The strains used in this paper are listed in Table 2. Yeast cells were cultured in YPD (1% yeast extract, 2% peptone, and 2% dextrose), synthetic defined (SD) or synthetic complete (SC) (0.17% yeast nitrogen base without amino acids and ammonium sulfate, 0.5% ammonium sulfate, and 2% dextrose with appropriate amino acids and bases as necessary). Cells were cultured at 30$^{o}$C and 250 rpm. 5-Fluoroorotic acid (5-FOA; ZYMO RESEARCH F9003), or doxycycline (Sigma D9891), were included as indicated. YPO (1% yeast extract, 2% peptone, 0.1% dextrose, 0.125% oleic acid, 0.5% Tween80) medium was used to induce lipid droplet formation.

Strain KSY512 was generated from a heterozygous *rft1::KANMX4* / *RFT1* deficient strain (YAKM158) which was transformed with p416-$P_{GPD}$-hRft1-3xFLAG(EcAKM135) and sporulated. Individual spores were obtained by tetrad analysis and colonies, initially grown on YPD, were tested for growth on YPD+G418 and SD(-Ura) plates. The disruption of genomic *RFT1* in KSY512 was also checked by PCR with *KANMX4*-specific primers.

YAKM223(mCherry-HDEL) and YAKM164($P_{tet}$-RFT1 Nvj1-nB $P_{ADH}$-AFLA-mNG-hRFT1) were created by transforming S288C or YAKM163 yeast strains with EcAKM153 and EcAKM154 plasmids, respectively, digested with AscI. After transformation, colonies were selected by SD(-Leu) plate.

To integrate ALFA-mNG-hRft1-3xFLAG and point mutants under control of GPD, TEF or ADH promoters into different yeast strains (YAKM223, ATY502, YAKM147), the cells were transformed with plasmids EcAKM150-152,164-167 that were linearized with NotI. After integration, colonies were selected on YPD containing 300 µg/ml hygromycin B (Gibco 10-687-010).

## Yeast growth assay

For plate assays, cells were adjusted to $OD_{600}$=1.0 and 10-fold serial dilutions were spotted. Plates were incubated at 30˚C for 2-3 days before being photographed. For generating growth curves, cells were cultured in SD(-His) medium to mid-log phase and diluted to $OD_{600}$=0.01 in a 96-well plate. The plate was covered with a Breathe-Easy® polyurethane sealing membrane (Sigma Z380059) and placed in a SpectraMax i3x plate reader (Molecular Devices), incubated at 30$^{o}$C, and $OD_{600}$ was measured every 15 min for 36 h. The plate was shaken for 5 sec before each measurement. Doubling time was calculated as $(t_2-t_1) \times \log2/(\log C_2-\log C_1)$, where the $OD_{600}$ of the

culture at times $t_1$ and $t_2$ correspond to $C_1$ and $C_2$, respectively. The values of $C_1$ and $C_2$ were chosen to be $\geq$0.35 and $\leq$0.5, respectively.

### SDS-PAGE immunoblotting

Cells were cultured to mid-log phase, and 2 $OD_{600}$ units were collected. The cells were lysed in 0.28 ml 0.2 M NaOH, 0.5% β-mercaptoethanol and incubated on ice for 5 min before adding 1 ml 15% TCA to precipitate all proteins. After 10 min incubation on ice, precipitated proteins were collected by centrifugation (14,000 rpm, 5 min, 4°C), washed with 0.6 ml ice-cold acetone, air-dried, and solubilized overnight in 0.2 ml 2% SDS, 5 mM NaOH, 2% β-mercaptoethanol. The samples were mixed with 100 μl of 2xSDS-PAGE loading buffer and used for SDS-PAGE. CPY, Dpm1, and FLAG were detected by immunoblotting with primary anti-CPY (1:5000; Invitrogen 10A5B5), anti-Dpm1 (1:1000; Life technology 5C5A7)), or anti-FLAG (1:2000; Sigma F1804) antibodies, followed by HRP-conjugated secondary anti-mouse antibody (1:5000, Promega W402B), diluted as indicated. Images were captured on an Odyssey XF (LI-COR) and band intensities were calculated using Image Studio software (LI-COR).

CPY glycosylation score calculation was described previously (29). Briefly, the intensities of each CPY band were quantified using Image Studio software, and the data set was used to calculate the CPY Glycoscore. The relative intensities of bands were multiplied by 4, 3, 2, 1, and 0, representing fully glycosylated CPY, and lacking 1, 2, 3, and 4 *N*-glycans, respectively. Values were summed, divided by 400, and converted to percentages.

### Fluorescence microscopy

Cells were cultured in YPD medium to mid-log phase, harvested, washed with water, and collected by centrifugation at room temperature in a microcentrifuge. To induce lipid droplet formation, mid-log phase cells were harvested and washed with YPO medium. Cells were resuspended with YPO medium and incubated at 30°C for 16 hours, then washed with water and collected by centrifugation at room temperature in a microcentrifuge. Cells were imaged using an LSM 880 Confocal Laser Scanning Microscope (Zeiss) with ZEN Microscopy software (Zeiss), and 488 nm and 514 nm lasers for mNG and mCherry, respectively. For grayscale images, acquired images were processed with the ImageJ software. Select “Images > Lookup tables > Grays” and “Edit > Invert” to convert the images to grayscale.

### Preparation of yeast microsomes and the Triton Extract (TE)

Salt-washed microsomes were prepared from a homogenate of KSY512 yeast cells as described previously (21), except an additional centrifugation step (20,000 × $g_{av}$, 30 min, 4°C) was included after the initial low-speed spin to clear the homogenate of mitochondria, assessed by immunoblotting to detect Por1, the mitochondrial outer membrane porin. The salt-washed microsomes were incubated with ice-cold Triton X-100 as previously described (21) to generate a Triton extract (TE, buffer composition: 50 mM Hepes, pH 7.4, 150 mM NaCl, 1% (w/v) Triton X-100) selectively enriched in ER membrane proteins (5). hRft1-3xFLAG was quantitatively eliminated from the TE by incubating the extract (300 μl) with anti-FLAG M2 affinity gel resin (Sigma A220; bed volume 100 μl); an equivalent aliquot of TE was mock-treated in parallel. Specific elimination of hRft1-3xFLAG was confirmed by immunoblotting with anti-FLAG and anti-Dpm1

antibodies as described above. The protein concentration of the TE, irrespective of treatment, was ~0.5 mg/ml as determined by the Pierce Micro BCA Protein Assay kit (ThermoFisher 23235).

## Reconstitution of proteoliposomes and scramblase assays

Proteoliposomes and protein-free liposomes were reconstituted using a previously described one-pot protocol (21) with some modifications. Briefly, to prepare three reconstituted samples, 10 mg egg phosphatidylcholine (Avanti Polar Lipids 840051), 45 μg 16:0-06:0 NBD-PC (Avanti Polar Lipids 810130C) and ~40,000 cpm [$^3$H]M5-DLO (21) were added from chloroform or chloroform/methanol stock solutions to a glass tube, dried under a stream of nitrogen, dissolved in 1 ml pentane (Sigma 34956-1L) and dried again under nitrogen. The resulting lipid film was dissolved to clarity by stepwise addition of 10/100/1 buffer (10 mM Hepes, pH 7.4, 100 mM NaCl, 1% (w/v) Triton X-100) to a total volume of 1.85 ml. The lipid solution was distributed into three 2-ml Eppendorf tubes (600 μl per tube) and supplemented with 400 μl of either 10/100/1 buffer, mock-treated TE, or α-FLAG-treated TE to generate protein-free liposomes, complete proteoliposomes, or Rft1-deficient proteoliposomes, respectively. The samples were incubated at room temperature with end-over-end mixing for 30 min before adding washed BioBeads SM2 (Bio-Rad 152-39120) in two stages. First, each sample received 100 mg BioBeads and was incubated with end-over-end mixing at room temperature for 3 h. Next, the samples were supplemented with 200 mg BioBeads and incubated with end-over-end mixing in a cold-room overnight (~15 h). The samples were removed from the BioBeads and centrifuged in a Beckman TLA100.2 rotor at 75,000 rpm (~250,000 x $g_{max}$)at 4°C for 1 h. The resulting membrane pellets were each resuspended in 200 μl MMC buffer (10 mM Hepes, pH 7.4, 100 mM NaCl, 3 mM $MgCl_2$,1 mM $MnCl_2$,1 mM $CaCl_2$). Aliquots of the resuspended pellets were taken for dynamic light scattering and phospholipid scramblase activity assays as described (45), and M5-DLO scramblase assay according to a standard protocol (21).

## Data availability

All data are contained within the manuscript.

## Supporting information

This article contains supporting information (Table 1-3, Figs. S1-S5).

## Acknowledgements

We thank the Optical Microscopy and Imaging services of the Microscopy & Image Analysis Core Facility at Weill Cornell, as well several individuals at Weill Cornell for use of their equipment: James Jordan and Baran Ersoy (plate reader), Beate Schwer (tetrad dissecting microscope), and David Simon (fluorescence microscope). We thank Ralf Erdmann, Roger Schneiter and Vineet Choudhary for advice on induction of lipid droplets in yeast and the following individuals for reagents: Alice Verchère for [$^3$H]M5-DLO, Maya Schuldiner (Weizmann Institute) for Tet-off strains, Alexandre Toulmay and Jonathan Friedman (University of Texas Southwestern Medical Center) for the Erg6-mCherry-expressing cells and the mCherry-HDEL plasmid, respectively, Bianca Esch and Florian Fröhlich (Osnabrück University) for reagents to carry out nanobody-based recruitment of Rft1 to ER domains, and Hiroki Okada (Erfei Bi laboratory, University of Pennsylvania) for integration plasmids.

## Funding and additional information

We acknowledge support from National Institutes of Health grants R21 HD109719 and R01 GM146011 (A.K.M.), and the Fonds National de la Recherche Scientifique (FRS-FNRS; Grant number 1.B.089.24F)(G.N.C.).

The content is solely the responsibility of the authors and does not necessarily represent the official views of the National Institutes of Health.

## Conflict of interest

The authors declare that they have no conflicts of interest with the contents of this article.

## REFERENCES


1. Ramirez, A. S., andLocher, K. P. (2023) Structural and mechanistic studies of the N-glycosylation machinery: From lipid-linked oligosaccharide biosynthesis to glycan transfer Glycobiology 10.1093/glycob/cwad053
2. Breitling, J., andAebi, M. (2013) N-linked protein glycosylation in the endoplasmic reticulum Cold Spring Harb Perspect Biol 5, a013359 10.1101/cshperspect.a013359
3. Sanyal, S., andMenon, A. K. (2009) Flipping lipids: why an' what's the reason for? ACS Chem Biol 4, 895-909 10.1021/cb900163d
4. Pomorski, T. G., andMenon, A. K. (2016) Lipid somersaults: Uncovering the mechanisms of protein-mediated lipid flipping Prog Lipid Res 64, 69-84 10.1016/j.plipres.2016.08.003
5. Sanyal, S., Frank, C. G., andMenon, A. K. (2008) Distinct flippases translocate glycerophospholipids and oligosaccharide diphosphate dolichols across the endoplasmic reticulum Biochemistry 47, 7937-7946 10.1021/bi800723n
6. Sanyal, S., andMenon, A. K. (2009) Specific transbilayer translocation of dolichol-linked oligosaccharides by an endoplasmic reticulum flippase Proc Natl Acad Sci U S A 106, 767-772 10.1073/pnas.0810225106
7. Schenk, B., Fernandez, F., andWaechter, C. J. (2001) The ins(ide) and out(side) of dolichyl phosphate biosynthesis and recycling in the endoplasmic reticulum Glycobiology 11, 61R-70R 10.1093/glycob/11.5.61r
8. Schachter, H. (2001) Congenital disorders involving defective N-glycosylation of proteins Cell Mol Life Sci 58, 1085-1104, http://www.ncbi.nlm.nih.gov/pubmed/11529501
9. McDowell, G., andGahl, W. A. (1997) Inherited disorders of glycoprotein synthesis: cell biological insights Proc Soc Exp Biol Med 215, 145-157, http://www.ncbi.nlm.nih.gov/pubmed/9160042
10. Freeze, H. H., andAebi, M. (2005) Altered glycan structures: the molecular basis of congenital disorders of glycosylation Curr Opin Struct Biol 15, 490-498 S0959-440X(05)00158-2 [pii]
10.1016/j.sbi.2005.08.010
11. Freeze, H. H., Eklund, E. A., Ng, B. G., andPatterson, M. C. (2012) Neurology of inherited glycosylation disorders Lancet Neurol 11, 453-466 10.1016/S1474-4422(12)70040-6
S1474-4422(12)70040-6 [pii]
12. Freeze, H. H. (2013) Understanding human glycosylation disorders: biochemistry leads the charge J Biol Chem 288, 6936-6945 10.1074/jbc.R112.429274
R112.429274 [pii]
13. Freeze, H. H., Chong, J. X., Bamshad, M. J., andNg, B. G. (2014) Solving glycosylation disorders: fundamental approaches reveal complicated pathways Am J Hum Genet 94, 161-175 10.1016/j.ajhg.2013.10.024
S0002-9297(13)00481-3 [pii]
14. Haeuptle, M. A., Pujol, F. M., Neupert, C., Winchester, B., Kastaniotis, A. J., Aebi, M. et al. (2008) Human RFT1 deficiency leads to a disorder of N-linked glycosylation Am J Hum Genet 82, 600-606 10.1016/j.ajhg.2007.12.021

15. Vleugels, W., Haeuptle, M. A., Ng, B. G., Michalski, J. C., Battini, R., Dionisi-Vici, C. et al. (2009) RFT1 deficiency in three novel CDG patients Hum Mutat 30, 1428-1434 10.1002/humu.21085
16. Jaeken, J., Vleugels, W., Regal, L., Corchia, C., Goemans, N., Haeuptle, M. A. et al. (2009) RFT1-CDG: deafness as a novel feature of congenital disorders of glycosylation J Inherit Metab Dis 32 Suppl 1, S335-338 10.1007/s10545-009-1297-3
17. Helenius, J., Ng, D. T., Marolda, C. L., Walter, P., Valvano, M. A., andAebi, M. (2002) Translocation of lipid-linked oligosaccharides across the ER membrane requires Rft1 protein Nature 415, 447-450 10.1038/415447a
18. Ng, D. T., Spear, E. D., andWalter, P. (2000) The unfolded protein response regulates multiple aspects of secretory and membrane protein biogenesis and endoplasmic reticulum quality control J Cell Biol 150, 77-88 10.1083/jcb.150.1.77
19. Helenius, J., andAebi, M. (2002) Transmembrane movement of dolichol linked carbohydrates during N-glycoprotein biosynthesis in the endoplasmic reticulum Semin Cell Dev Biol 13, 171-178 10.1016/s1084-9521(02)00045-9
20. Frank, C. G., Sanyal, S., Rush, J. S., Waechter, C. J., andMenon, A. K. (2008) Does Rft1 flip an N-glycan lipid precursor? Nature 454, E3-4; discussion E4-5 10.1038/nature07165
21. Verchere, A., Cowton, A., Jenni, A., Rauch, M., Haner, R., Graumann, J. et al. (2021) Complexity of the eukaryotic dolichol-linked oligosaccharide scramblase suggested by activity correlation profiling mass spectrometry Sci Rep 11, 1411 10.1038/s41598-020-80956-0
22. Rush, J. S., Gao, N., Lehrman, M. A., Matveev, S., andWaechter, C. J. (2009) Suppression of Rft1 expression does not impair the transbilayer movement of Man5GlcNAc2-P-P-dolichol in sealed microsomes from yeast J Biol Chem 284, 19835-19842 10.1074/jbc.M109.000893
23. Jelk, J., Gao, N., Serricchio, M., Signorell, A., Schmidt, R. S., Bangs, J. D. et al. (2013) Glycoprotein biosynthesis in a eukaryote lacking the membrane protein Rft1 J Biol Chem 288, 20616-20623 10.1074/jbc.M113.479642
24. Aebi, M., andHennet, T. (2001) Congenital disorders of glycosylation: genetic model systems lead the way Trends Cell Biol 11, 136-141 10.1016/s0962-8924(01)01925-0
25. Wach, A., Brachat, A., Pohlmann, R., andPhilippsen, P. (1994) New heterologous modules for classical or PCR-based gene disruptions in Saccharomyces cerevisiae Yeast 10, 1793-1808 10.1002/yea.320101310
26. Mumberg, D., Müller, R., andFunk, M. (1995) Yeast vectors for the controlled expression of heterologous proteins in different genetic backgrounds Gene 156, 119-122 10.1016/0378-1119(95)00037-7
27. Ho, B., Baryshnikova, A., andBrown, G. W. (2018) Unification of Protein Abundance Datasets Yields a Quantitative Saccharomyces cerevisiae Proteome Cell Syst 6, 192-205 e193 10.1016/j.cels.2017.12.004
28. Hasilik, A., andTanner, W. (1978) Carbohydrate moiety of carboxypeptidase Y and perturbation of its biosynthesis Eur J Biochem 91, 567-575 10.1111/j.1432-1033.1978.tb12710.x

29. Frey, A. D., andAebi, M. (2015) An enzyme-based screening system for the rapid assessment of protein N-glycosylation efficiency in yeast Glycobiology 25, 252-257 10.1093/glycob/cwu134
30. Shaner, N. C., Lambert, G. G., Chammas, A., Ni, Y., Cranfill, P. J., Baird, M. A. et al. (2013) A bright monomeric green fluorescent protein derived from Branchiostoma lanceolatum Nat Methods 10, 407-409 10.1038/nmeth.2413
31. Gotzke, H., Kilisch, M., Martinez-Carranza, M., Sograte-Idrissi, S., Rajavel, A., Schlichthaerle, T. et al. (2019) The ALFA-tag is a highly versatile tool for nanobody-based bioscience applications Nat Commun 10, 4403 10.1038/s41467-019-12301-7
32. Anand, M., Rush, J. S., Ray, S., Doucey, M. A., Weik, J., Ware, F. E. et al. (2001) Requirement of the Lec35 gene for all known classes of monosaccharide-P-dolichol-dependent glycosyltransferase reactions in mammals Mol Biol Cell 12, 487-501 10.1091/mbc.12.2.487
33. Schenk, B., Imbach, T., Frank, C. G., Grubenmann, C. E., Raymond, G. V., Hurvitz, H. et al. (2001) MPDU1 mutations underlie a novel human congenital disorder of glycosylation, designated type If J Clin Invest 108, 1687-1695 10.1172/JCI13419
34. Krahmer, N., Hilger, M., Kory, N., Wilfling, F., Stoehr, G., Mann, M. et al. (2013) Protein correlation profiles identify lipid droplet proteins with high confidence Mol Cell Proteomics 12, 1115-1126 10.1074/mcp.M112.020230
35. Bickel, T., Lehle, L., Schwarz, M., Aebi, M., andJakob, C. A. (2005) Biosynthesis of lipid-linked oligosaccharides in Saccharomyces cerevisiae: Alg13p and Alg14p form a complex required for the formation of GlcNAc(2)-PP-dolichol J Biol Chem 280, 34500-34506 10.1074/jbc.M506358200
36. Chantret, I., Dancourt, J., Barbat, A., andMoore, S. E. (2005) Two proteins homologous to the N- and C-terminal domains of the bacterial glycosyltransferase Murg are required for the second step of dolichyl-linked oligosaccharide synthesis in Saccharomyces cerevisiae J Biol Chem 280, 9236-9242 10.1074/jbc.M413941200
37. Gao, X. D., Tachikawa, H., Sato, T., Jigami, Y., andDean, N. (2005) Alg14 recruits Alg13 to the cytoplasmic face of the endoplasmic reticulum to form a novel bipartite UDP-N-acetylglucosamine transferase required for the second step of N-linked glycosylation J Biol Chem 280, 36254-36262 10.1074/jbc.M507569200
38. Olarte, M. J., Kim, S., Sharp, M. E., Swanson, J. M. J., Farese, R. V., Jr., andWalther, T. C. (2020) Determinants of Endoplasmic Reticulum-to-Lipid Droplet Protein Targeting Dev Cell 54, 471-487 e477 10.1016/j.devcel.2020.07.001
39. Olarte, M. J., Swanson, J. M. J., Walther, T. C., andFarese, R. V., Jr. (2022) The CYTOLD and ERTOLD pathways for lipid droplet-protein targeting Trends Biochem Sci 47, 39-51 10.1016/j.tibs.2021.08.007
40. Mishra, S., Khaddaj, R., Cottier, S., Stradalova, V., Jacob, C., andSchneiter, R. (2016) Mature lipid droplets are accessible to ER luminal proteins J Cell Sci 129, 3803-3815 10.1242/jcs.189191
41. Leber, R., Zinser, E., Zellnig, G., Paltauf, F., andDaum, G. (1994) Characterization of lipid particles of the yeast, Saccharomyces cerevisiae Yeast 10, 1421-1428 10.1002/yea.320101105

42. Esch, B. M., Walter, S., Schmidt, O., andFrohlich, F. (2023) Identification of distinct active pools of yeast serine palmitoyltransferase in sub-compartments of the ER J Cell Sci 136, 10.1242/jcs.261353
43. Vehring, S., Pakkiri, L., Schroer, A., Alder-Baerens, N., Herrmann, A., Menon, A. K. et al. (2007) Flip-flop of fluorescently labeled phospholipids in proteoliposomes reconstituted with Saccharomyces cerevisiae microsomal proteins Eukaryot Cell 6, 1625-1634 10.1128/EC.00198-07
44. Menon, A. K., Watkins, W. E. r., andHrafnsdottir, S. (2000) Specific proteins are required to translocate phosphatidylcholine bidirectionally across the endoplasmic reticulum Curr Biol 10, 241-252 10.1016/s0960-9822(00)00356-0
45. Menon, I., Sych, T., Son, Y., Morizumi, T., Lee, J., Ernst, O. P. et al. (2024) A cholesterol switch controls phospholipid scrambling by G protein-coupled receptors J Biol Chem 300, 105649 10.1016/j.jbc.2024.105649
46. Chalat, M., Menon, I., Turan, Z., andMenon, A. K. (2012) Reconstitution of glucosylceramide flip-flop across endoplasmic reticulum: implications for mechanism of glycosphingolipid biosynthesis J Biol Chem 287, 15523-15532 10.1074/jbc.M112.343038
47. Jumper, J., Evans, R., Pritzel, A., Green, T., Figurnov, M., Ronneberger, O. et al. (2021) Highly accurate protein structure prediction with AlphaFold Nature 596, 583-589 10.1038/s41586-021-03819-2
48. Varadi, M., Anyango, S., Deshpande, M., Nair, S., Natassia, C., Yordanova, G. et al. (2022) AlphaFold Protein Structure Database: massively expanding the structural coverage of protein-sequence space with high-accuracy models Nucleic Acids Res 50, D439-D444 10.1093/nar/gkab1061
49. Hallgren, J., Tsirigos, K. D., Pedersen, M. D., Armenteros, J. J. A., Marcatili, P., Nielsen, H. et al. (2022) DeepTMHMM predicts alpha and beta transmembrane proteins using deep neural networks bioRxiv https://doi.org/10.1101/2022.04.08.487609
50. Sanyal, S., andMenon, A. K. (2010) Stereoselective transbilayer translocation of mannosyl phosphoryl dolichol by an endoplasmic reticulum flippase Proc Natl Acad Sci U S A 107, 11289-11294 10.1073/pnas.1002408107
51. Zimmermann, L., Stephens, A., Nam, S. Z., Rau, D., Kubler, J., Lozajic, M. et al. (2018) A Completely Reimplemented MPI Bioinformatics Toolkit with a New HHpred Server at its Core J Mol Biol 430, 2237-2243 10.1016/j.jmb.2017.12.007
52. Hvorup, R. N., Winnen, B., Chang, A. B., Jiang, Y., Zhou, X. F., andSaier, M. H., Jr. (2003) The multidrug/oligosaccharidyl-lipid/polysaccharide (MOP) exporter superfamily Eur J Biochem 270, 799-813 10.1046/j.1432-1033.2003.03418.x
53. Zheng, S., Sham, L. T., Rubino, F. A., Brock, K. P., Robins, W. P., Mekalanos, J. J. et al. (2018) Structure and mutagenic analysis of the lipid II flippase MurJ from Escherichia coli Proc Natl Acad Sci U S A 115, 6709-6714 10.1073/pnas.1802192115
54. Kuk, A. C. Y., Hao, A., andLee, S. Y. (2022) Structure and Mechanism of the Lipid Flippase MurJ Annu Rev Biochem 91, 705-729 10.1146/annurev-biochem-040320-105145
55. Kumar, S., Rubino, F. A., Mendoza, A. G., andRuiz, N. (2019) The bacterial lipid II flippase MurJ functions by an alternating-access mechanism J Biol Chem 294, 981-990 10.1074/jbc.RA118.006099

56. Rubino, F. A., Kumar, S., Ruiz, N., Walker, S., andKahne, D. E. (2018) Membrane Potential Is Required for MurJ Function J Am Chem Soc 140, 4481-4484 10.1021/jacs.8b00942
57. Ashkenazy, H., Abadi, S., Martz, E., Chay, O., Mayrose, I., Pupko, T. et al. (2016) ConSurf 2016: an improved methodology to estimate and visualize evolutionary conservation in macromolecules Nucleic Acids Res 44, W344-350 10.1093/nar/gkw408
58. Landau, M., Mayrose, I., Rosenberg, Y., Glaser, F., Martz, E., Pupko, T. et al. (2005) ConSurf 2005: the projection of evolutionary conservation scores of residues on protein structures Nucleic Acids Res 33, W299-302 10.1093/nar/gki370
59. Nicoludis, J. M., andGaudet, R. (2018) Applications of sequence coevolution in membrane protein biochemistry Biochim Biophys Acta Biomembr 1860, 895-908 10.1016/j.bbamem.2017.10.004
60. Anishchenko, I., Ovchinnikov, S., Kamisetty, H., andBaker, D. (2017) Origins of coevolution between residues distant in protein 3D structures Proc Natl Acad Sci U S A 114, 9122-9127 10.1073/pnas.1702664114
61. Choi, Y., Sims, G. E., Murphy, S., Miller, J. R., andChan, A. P. (2012) Predicting the functional effect of amino acid substitutions and indels PLoS One 7, e46688 10.1371/journal.pone.0046688
62. Samuelson, J., Banerjee, S., Magnelli, P., Cui, J., Kelleher, D. J., Gilmore, R. et al. (2005) The diversity of dolichol-linked precursors to Asn-linked glycans likely results from secondary loss of sets of glycosyltransferases Proc Natl Acad Sci U S A 102, 1548-1553 10.1073/pnas.0409460102
63. Sham, L. T., Butler, E. K., Lebar, M. D., Kahne, D., Bernhardt, T. G., andRuiz, N. (2014) Bacterial cell wall. MurJ is the flippase of lipid-linked precursors for peptidoglycan biogenesis Science 345, 220-222 10.1126/science.1254522
64. Rush, J. S., andWaechter, C. J. (1995) Transmembrane movement of a water-soluble analogue of mannosylphosphoryldolichol is mediated by an endoplasmic reticulum protein J Cell Biol 130, 529-536 10.1083/jcb.130.3.529

## Footnotes

The abbreviations used are: 5-FOA, 5-fluoroorotic acid; CDG, congenital disorder of glycosylation; CPY, carboxypeptidase Y; DDM, n-dodecyl-β-maltoside; DLO, dolichol-linked oligosaccharide; DLS, dynamic light scattering; Dox, doxycyline; ECL, extracellular loop; ER, endoplasmic reticulum; G3M9-DLO, Glucose$_3$Mannose$_9$GlcNAc$_2$-diphosphate-dolichol; Glc, glucose; GlcNAc, *N*-acetylglucosamine; GPD, strong, constitutively active promoter from glyceraldehyde 3-phosphate dehydrogenase; His, histidine; hRft1, human Rft1; LUV, large unilamellar vesicle; M5-DLO, Mannose$_5$GlcNAc$_2$-diphosphate-dolichol; Man, mannose; mCPY, mature CPY; mNG, mNeonGreen; NBD, 7-nitro-2,1,3-benzoxadiazole; OST, oligosaccharyltransferase; PC, phosphatidylcholine; SD medium, synthetic defined medium; TE, Triton X-100 Extract enriched in ER membrane proteins; Ura, uracil

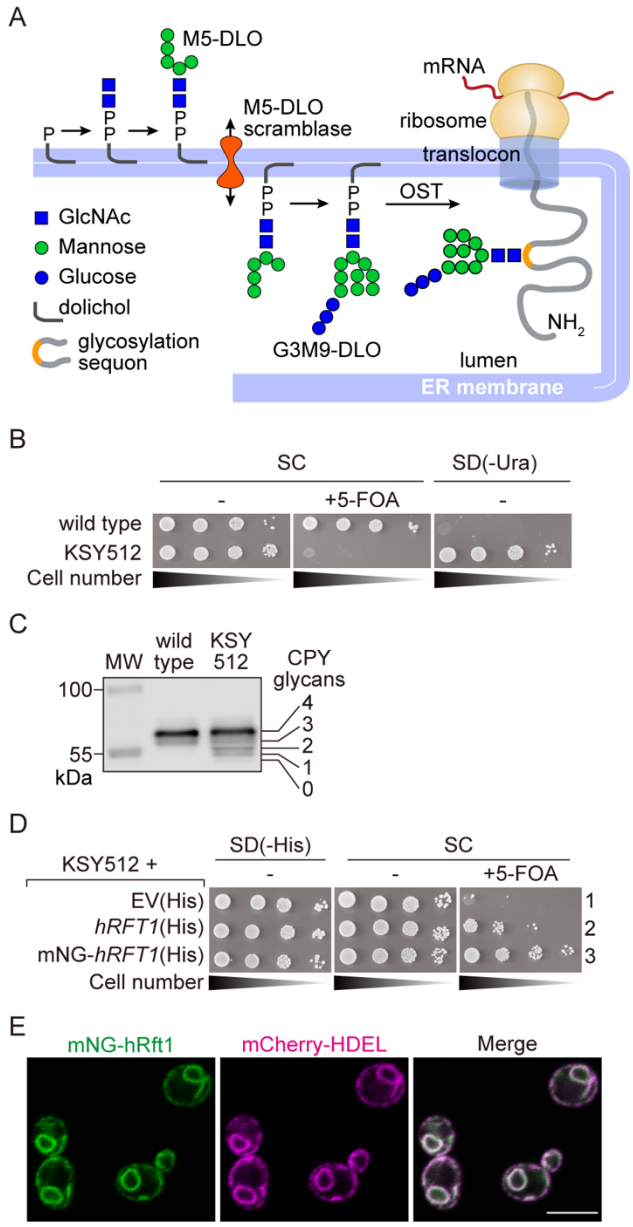


Figure 1. Functional replacement of yeast Rft1 by human Rft1.

**A.** Protein *N*-glycosylation in the ER. $Glc_3Man_9GlcNAc_2$-PP-dolichol (G3M9-DLO), the oligosaccharide donor for protein *N*-glycosylation in yeast and humans, is synthesized in two stages. The first stage produces $Man_5GlcNAc_2$-PP-dolichol (M5-DLO) on the cytoplasmic side of the ER. M5-DLO then moves across the membrane to the luminal side (a process facilitated by M5-DLO scramblase) where it is converted to G3M9-DLO. Oligosaccharyltransferase (OST) transfers the G3M9 oligosaccharide from G3M9-DLO to a glycosylation sequon (NXS/T, single letter amino acid code, where X is any amino acid except proline) in a nascent protein as it emerges from the protein translocon into the ER lumen.

**B.** Serial 10-fold dilutions of wild-type (BY4741) and KSY512 cells were spotted on SC plates +/- 5-FOA and SD(-Ura) and incubated at 30°C for 3 days.

**C.** Wild-type (BY4741) and KSY512 cells were cultured in YPD liquid medium to log-phase, harvested and analyzed by SDS-PAGE and immunoblotting with anti-CPY antibody. The annotation on the right indicates migration of mature CPY (with 4 *N*-glycans), and hypoglycosylated forms.
**D.** KSY512 cells, transformed with empty vector (EV, p413-$P_{GPD}$), $P_{GPD}$-hRFT1 and $P_{GPD}$-mNG-ALFA-hRFT1, were spotted (10-fold serial dilutions) on the indicated media and photographed after incubation at 30°C for 3 days.
**E.** The mNG-hRft1 construct (expression driven by the GPD promoter) was integrated into wild-type cells expressing the luminal ER marker mCherry-HDEL. The resulting $P_{GPD}$-mNG-*hRFT1* mCherry-HDEL cells were cultured in YPD medium to log-phase and imaged by confocal fluorescence microscopy. Scale bar = 5 μm.

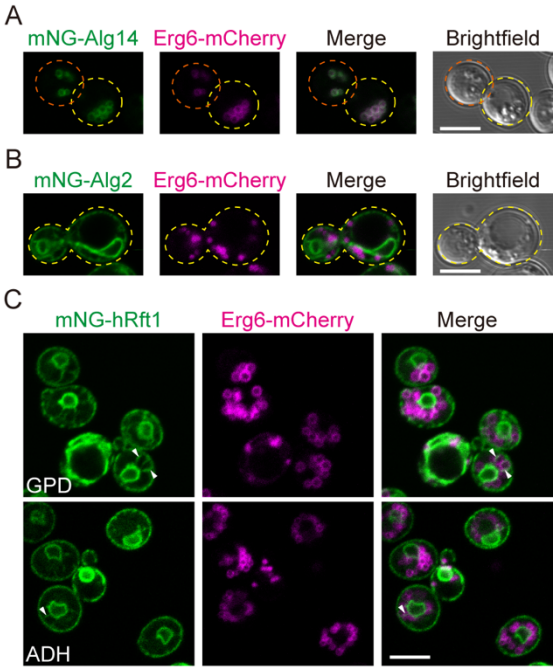


Figure 2. Alg14 co-localizes with lipid droplets, but Alg2 and Rft1 do not.

**A.** Erg6-mCherry cells carrying an mNG-Alg14 expressing plasmid were cultured in YPO medium for 16 h and visualized by confocal fluorescence microscopy. The dotted line indicates the shape of the cells.

**B.** As in panel A, except that the cells contained an mNG-Alg2 expressing plasmid.

**C.** $P_{GPD}$-mNG-*hRFT1* Erg6-mCherry and $P_{ADH}$-mNG-*hRFT1* Erg6-mCherry cells were cultured with YPO medium for 16 hours and visualized by confocal fluorescence microscopy. Arrowheads indicate mNG-hRft1-containing ER strands. Scale bar = 5 μm for all panels.

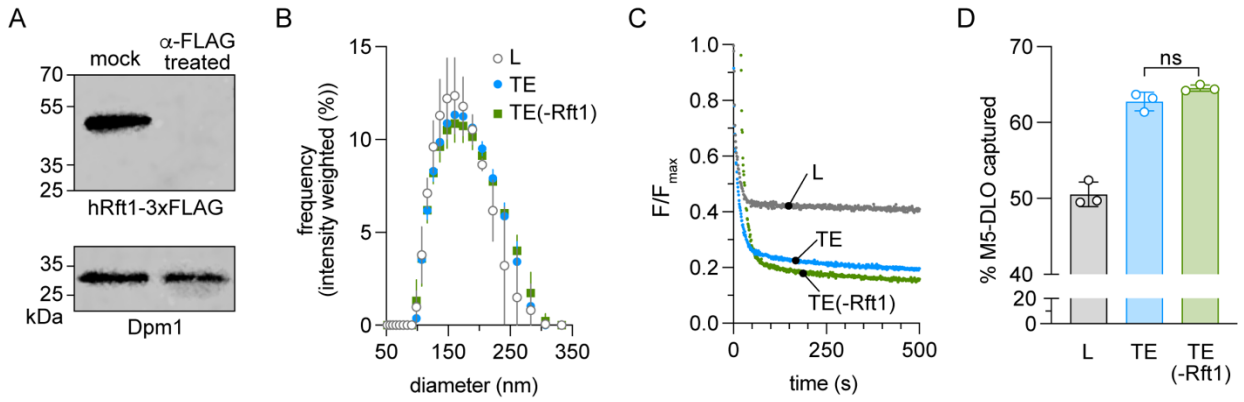


## Figure 3. Rft1 is not necessary for M5-DLO scrambling in vesicles reconstituted with yeast ER membrane proteins.

Microsomes were prepared by differential centrifugation of a homogenate of KSY512 cells, and salt-washed to remove peripheral proteins. The salt-washed membranes were extracted with ice-cold Triton X-100 to solubilize ER membrane proteins. The Triton extract (TE) was mock-treated or incubated with anti-FLAG resin to eliminate hRft1-3xFLAG, then reconstituted with egg phosphatidylcholine and trace quantities of NBD-PC and [$^3$H]M5-DLO to generate large unilamellar proteoliposomes (indicated as 'TE' and 'TE(-Rft1)') for scramblase activity assays. The protein/phospholipid ratio of the proteoliposomes was ~45 mg/mmol, based on input values of protein and phospholipid. Protein-free liposomes (L) were prepared in parallel.

**A.** Immunoblot using anti-FLAG (top) and anti-Dpm1 (bottom) antibodies. Identical cell equivalents were loaded in the mock-treated and anti-FLAG resin-treated samples. No FLAG signal was detected in the anti-FLAG resin-treated sample even upon loading 10-times more sample (not shown).

**B.** Diameter of reconstituted vesicles measured by dynamic light scattering. Error bars=mean ± S.D. (n=3).

**C.** NBD-PC scramblase activity assay. Dithionite was added at t=0 s and fluorescence (F) was monitored over time. The TE and TE(-Rft1) traces ($F/F_{max}$, normalized to the average fluorescence ($F_{max}$) prior to dithionite addition) overlap exactly; to improve visualization, the TE(-Rft1) trace is displaced downwards (0.05 y-units) and to the right (20 x-units).

**D.** M5-DLO scramblase activity assay. The y-axis indicates the fraction of [$^3$H]M5-DLO in the reconstituted vesicles that is captured by exogenously added Con A. For liposomes, the % capture is predicted to be 50%; for proteoliposomes with M5-DLO scramblase activity, the capture efficiency increases, the exact amount depending on the fraction of vesicles that has scramblase activity. See text for details. Error bars=mean ± S.D. (n=3); ns, no significant difference using ordinary one-way ANOVA.

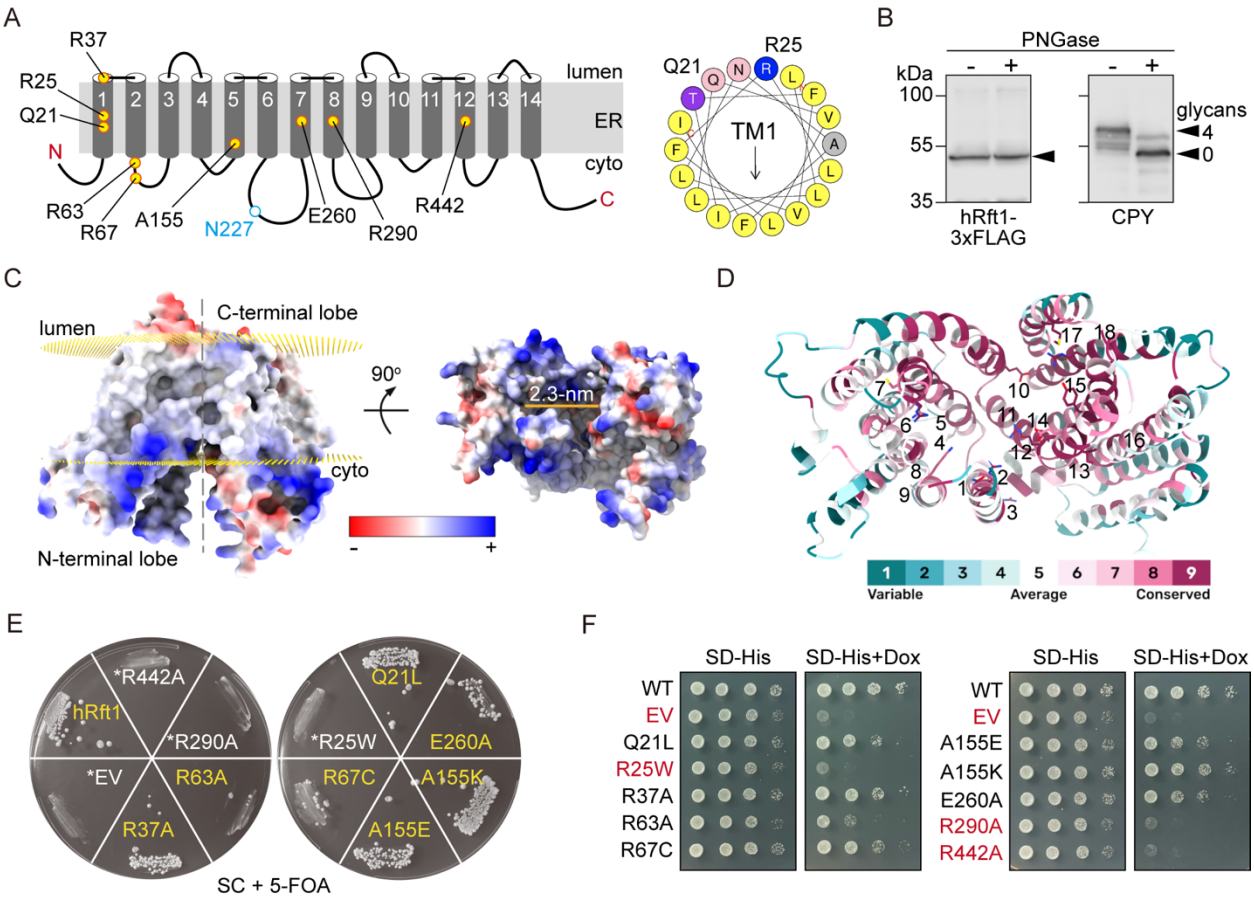


Figure 4. Functional architecture of Rft1.

**A.** Topology model of hRft1. The model is based on DeepTMHMM (https://dtu.biolib.com/DeepTMHMM) which predicts 14 transmembrane spans. The protein has its N- and C-terminus oriented towards the cytoplasm. The only *N*-glycosylation sequon ($N^{227}$IT) is located in the third intracellular loop. The relative lengths of the loops are shown roughly to scale. Sites that were mutated in this study are indicated by yellow circles. To the right of the model is a helical wheel depiction of TM1 generated using HeliQuest (https://heliquest.ipmc.cnrs.fr/cgi-bin/ComputParams.py).

**B.** hRft1 is not *N*-glycosylated. A protein extract from KSY512 cells was treated with PNGase F (a control sample was mock-treated in parallel) and subsequently analyzed by SDS-PAGE immunoblotting using anti-FLAG antibodies (to detect hRft1) and anti-CPY antibodies. Left panel, arrowhead indicates migration of hRft1. Right panel, arrowheads indicate the positions of fully glycosylated (4 glycans) and non-glycosylated (0 glycans) CPY; tick marks represent the same molecular weight markers as shown in the left panel.

**C.** Isosurface of the AlphaFold model of hRFT1 colored by electrostatics. Position of the lipid bilayer is shown as golden lattices on the left with the luminal side on top and the cytosolic side below as indicated. The structure can be divided (grey dashed line) into two lobes each containing 7 of the 14 TM. The width of the hydrophilic cavity between the lobes is ~23 Å as measured along the indicated gold line in the right view.

**D.** Cytosolic view of the hRFT1 model colored by ConSurf grade, with higher values indicating greater conservation as indicated in the color bar. CDG-1N associated residues (Table 3) and residues mutated and analyzed in this study are indicated by the numbers (1=Q21, 2=R25, 3=R37, 4=I43, 5=R63, 6=R67, 7=C70, 8=K152, 9+A155, 10=E260, 11=G276, 12=R290, 13=I296, 14=E298, 15=Y301, 16=G340, 17=M408, 18=R442).

**E.** KSY512 cells were transformed with *HIS3* plasmids for expression of hRft1 point mutants with a C-terminal 3xFLAG tag. Colonies picked from SD(-Ura, -His) plates were streaked onto plates containing 5-FOA (1 mg/ml) to eject the *URA3* plasmid carrying the hRFT1 gene. Images were taken after 3 days of incubation at 30°C. The hRft1 mutants that did not grow on the 5-FOA plate are marked with an asterisk and indicated in white; mutants that enabled growth are indicated in yellow.
**F.** A $P_{tet}$-*RFT1* strain was transformed with *HIS3* plasmids encoding hRft1 point mutants. A wildtype hRft1 (WT) construct and empty vector (EV) were also transformed into the cells as controls. Serial 10-fold dilutions of strains were spotted on SD (-His) +/- Dox (5 μg/ml) and incubated at 30°C for 2 days. Mutants that failed to support growth on Dox are labeled in red.

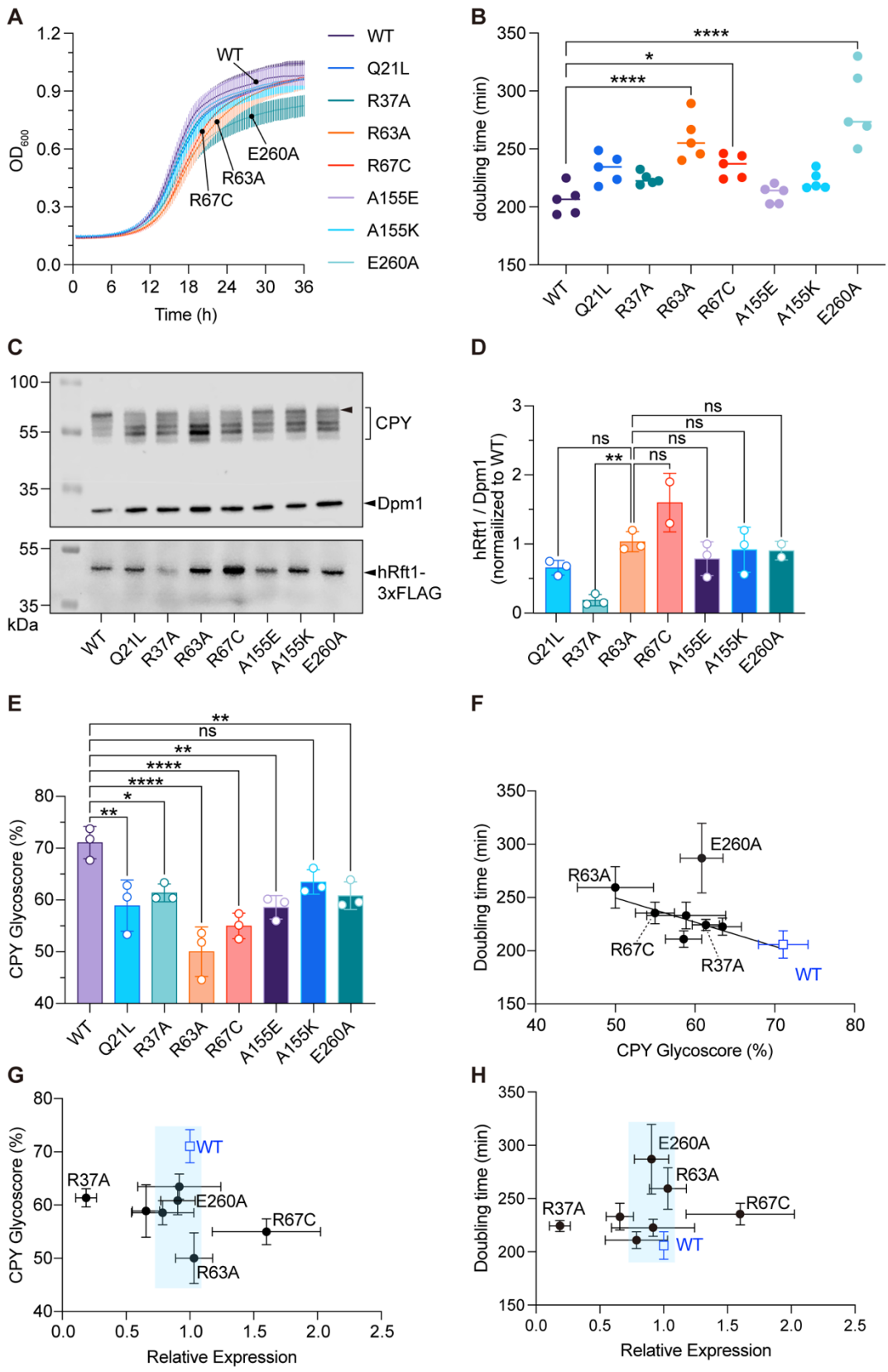


Figure 5. Analysis of cells expressing hRft1 point mutants.

Plasmid shuffling was used to replace the hRft1-expressing *URA3* plasmid in KSY512 cells with *HIS3* plasmids expressing wildtype hRft1-3xFLAG or corresponding point mutants.

**A.** KSY512 cells expressing hRft1-3xFLAG variants were cultured in SD(-His) medium to mid-log phase and diluted to $OD_{600}$=0.01. $OD_{600}$ was measured every 15 min for 36 h in a plate reader. Data are presented as mean ± S.D. (n=5).

**B.** Doubling time was determined from the exponential phase of the growth curves. Data are shown as a scatter dot plot, with a line indicating the median (n=5)(*p=0.0340, ****p<0.0001, all other pairs not significantly different, ordinary one-way ANOVA).

**C.** KSY512 cells expressing hRft1 point mutants were cultured in SD (-His) medium to log-phase, harvested, and analyzed by SDS-PAGE and immunoblotting with anti-CPY, anti-Dpm1, and anti-FLAG antibodies. The arrowhead in the CPY blot indicates fully glycosylated CPY.

**D.** hRft1-3xFLAG protein expression levels were quantified using data shown in panel C, combined with two additional biologically independent replicates (n=3). The ratio of the intensity of the hRft1-3xFLAG band to Dpm1 was calculated and normalized to that of the WT sample. Data are presented as mean ± S.D. (**p=0.003, ns, not significant, ordinary one-way ANOVA).

**E.** The intensity of each CPY band in panel C (together with two additional biologically independent replicates (n=3)) was analyzed and quantified to obtain the CPY Glycoscore. Data are presented as mean ± S.D. (*p=0.0113, **p=0.0017 (Q21L), 0.0013 (A155E), 0.0076 (E260A), ****p<0.0001, ordinary one-way ANOVA.).

**F.** Correlation between doubling time and CPY Glycoscore. Data points are mean ± S.D.

**G.** Correlation between CPY Glycoscore and expression. Data points are mean ± S.D.

**H.** Correlation between doubling time and expression. Data points are mean ± S.D.

**G-H.** The light blue shaded box is centered on the median of all expression values (x-axis) with a width +/- 20% of the median. The height of the box covers the y-axis data range.

Supporting Information

# Molecular characterization of Rft1, a membrane protein associated with congenital disorder of glycosylation type 1N

Eri Hirata[1‡], Ken-taro Sakata[1‡], Grace I. Dearden[1], Indu Menon[1], George N. Chiduza[2], Anant K. Menon[1]*

[1]Department of Biochemistry, Weill Cornell Medical College, New York, NY 10065, USA
[2]Structure and Function of Biological Membranes - Chemistry Department, Université Libre de Bruxelles - Campus Plaine, 1050 Brussels, Belgium

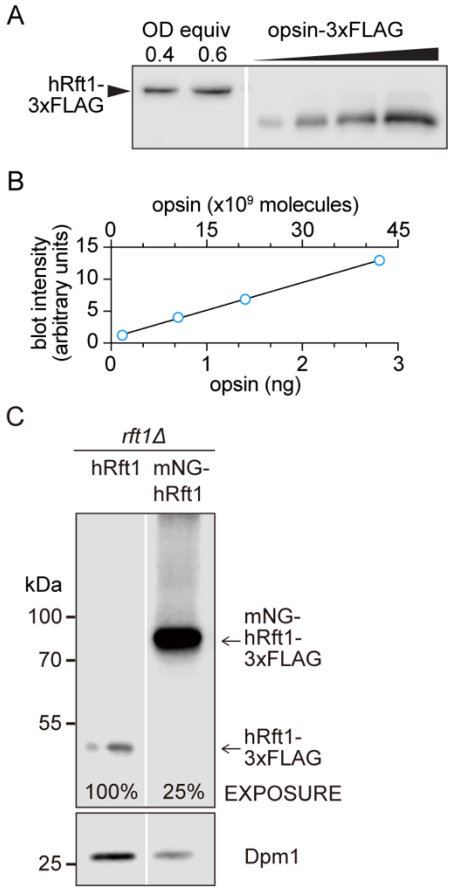


Supplementary Figure S1. Quantifying expression of hRft1 constructs.

**A.** KSY512 cells expressing hRft1-3xFLAG were cultured to a density of $OD_{600}$~1.1, and 2 OD600 units ($6x10^7$ cells) were collected. Cells were lysed in 0.28 ml 0.2 M NaOH, 0.5% β-mercaptoethanol, before adding 1 ml 15% TCA to precipitate all proteins. Precipitated proteins were washed with 0.6 ml ice-cold acetone and solubilized overnight in 2% SDS, 2% β-mercaptoethanol (neutralized with a small volume of NaOH). 20% and 30% of the total extract volume (0.4 and 0.6 OD equivalents) were run alongside 3xFLAG-tagged bovine opsin standards (0.12, 0.70, 1.4, and 2.8 ng (obtained by diluting a 117 ng/µL stock solution)(Ploier et al. (2016) Nat Commun 7, 12832) and visualized by immunoblotting with α-FLAG antibodies. The vertical white line separates portions of the same gel/blot. The opsin band runs just above the 35 kDa molecular weight marker; Rft1 runs between the 55 and 35 kDa markers (see Fig. 3B or Fig. 4A, for example).

**B.** The immunoblot signal intensity for the opsin standards (obtained by densitometry using ImageJ) was graphed against the protein amount loaded onto the gel (bottom x-axis), and linear regression was used to obtain a calibration plot. The x-axis at the top of the plot was obtained by converting opsin mass to number of molecules using a molecular weight of 40,000 g/mole. This plot was used to convert the Rft1 signal intensity (3.8 and 5.1 units (obtained using ImageJ), corresponding to 0.4 and 0.6 OD equivalents, respectively) to number of molecules, yielding a final result of 840 ± 35 molecules/cell (n=2).

**C.** Expression of mNG-hRft1 versus hRft1. Plasmid shuffling was used to replace hRft1 with mNG-hRft1 in KSY512 cells. Protein samples were prepared as in panel A and analyzed by SDS-PAGE immunoblotting using anti-FLAG antibodies and anti-Dpm1 antibodies (loading control). To avoid saturation, the exposure time for the right lane was reduced to 25% compared to the left lane.

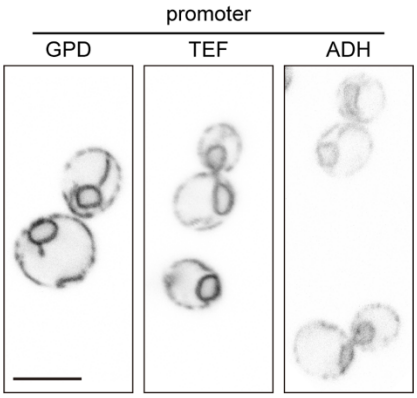


Supplementary Figure S2. Localization of mNG-hRft1 expressed under control of promoters of different strength.

The mNG-hRft1 construct was integrated into mCherry-HDEL-expressing wild-type cells, using three different promoters (GPD, TEF, ADH) to drive expression. The resulting cells ($P_{GPD}$-mNG-*hRFT1* mCherry-HDEL, $P_{TEF}$-mNG-*hRFT1* mCherry-HDEL, and $P_{ADH}$-mNG-*hRFT1* mCherry-HDEL) were cultured in YPD medium to log-phase and imaged by confocal fluorescence microscopy to visualize mNG-hRft1. Images were taken under the same conditions, using the same microscope settings. Promoter strength GPD>TEF>ADH. Scale bar = 5 μm

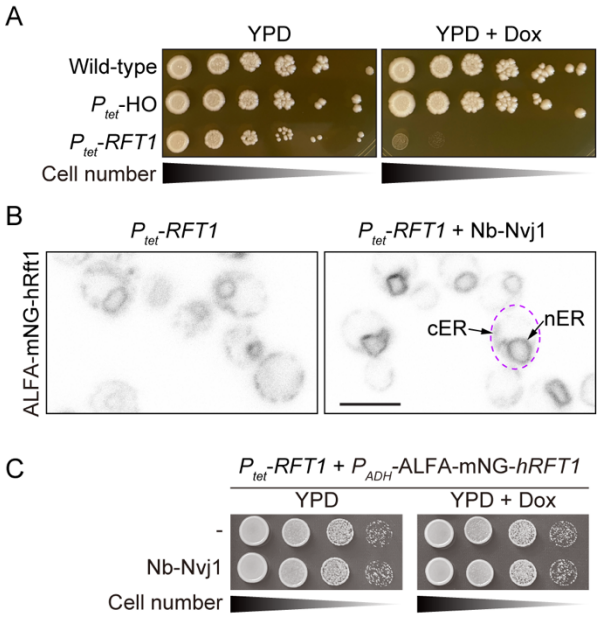


Supplementary Figure S3. Restriction of hRft1 to the nuclear ER does not affect function.

**A.** Serial 10-fold dilutions of wild-type (S288C), $P_{tet}$-HO (control for the Tet-off system), and $P_{tet}$-*RFT1* cells were spotted on YPD plates +/- Dox (5 μg/ml) and incubated at 30°C for 3 days.

**B.** $P_{tet}$-*RFT1* $P_{ADH}$ -ALFA-mNG-*hRFT1* and $P_{tet}$-*RFT1 NVJ1*-nB $P_{ADH}$-ALFA-mNG-*hRFT1* cells were cultured in YPD medium to log-phase and imaged by confocal fluorescence microscopy. The dotted line indicates the shape of the cell. The allows indicate cortical ER (cER) and nuclear ER (nER), respectively. Scale bar = 5 μm.

**C.** Serial 10-fold dilutions of $P_{tet}$-*RFT1* $P_{ADH}$ -ALFA-mNG-*hRFT1* and $P_{tet}$-*RFT1 NVJ1*-nB $P_{ADH}$-ALFA-mNG-*hRFT1* cells were spotted on YPD plates +/- Dox (5 μg/ml) and incubated at 30°C for 3 days.

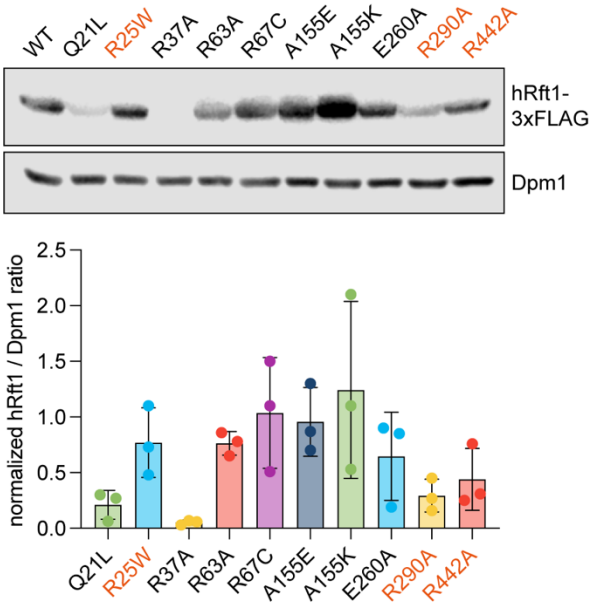


Supplementary Figure S4. Expression of hRft1 mutants.

**A.** (Left) wild type (BY4741) cells carrying *HIS3* plasmids for expression of hRft1 point mutants with a C-terminal 3xFLAG tag were cultured in SD(-His) medium and harvested. Immunoblot assay was performed using anti-FLAG and anti-Dpm1 antibodies. hRft1-3xFLAG and Dpm1 (loading control) were quantified from the immunoblot, and two additional biological replicates. The ratio of the intensity of the hRft1 band to Dpm1 was calculated and normalized to that of the WT sample (mean ± S.D., n=3). Pairwise comparisons (ordinary one-way ANOVA) with the R67 sample (chosen arbitrarily as the reference sample as it had an expression close to that of WT) showed no significant difference, except for R37 (p=0.0252).

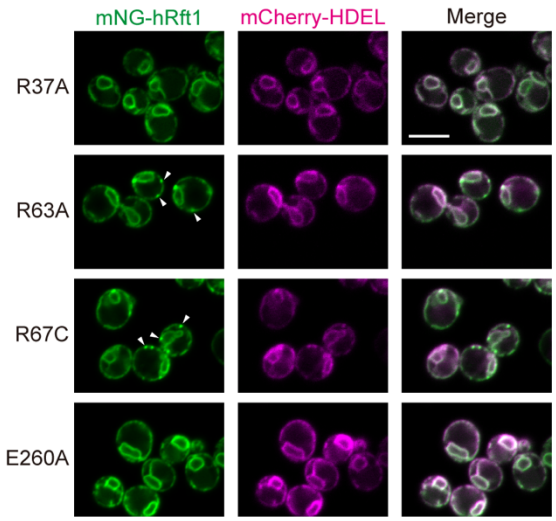


Supplementary Figure S5. Subcellular localization of hRft1 point mutants.

$P_{GPD}$-mNG-*hRFT1*$^{R37A/R63A/R67C/E260A}$ mCherry-HDEL cells (YAKM248-250, Table 2) were cultured in YPD medium to log-phase and imaged by confocal fluorescence microscopy. The arrowheads indicate hRft1 varicosities seen in the cortical ER (2, 50, 54 and 25% of R37A, R63A, R67C and E260A-expressing cells, respectively (n>100 cells counted in each case) displayed these varicosities). Scale bar = 5 μm.

Table 1. Plasmids

| PLASMID NAME | ALIAS | CONSTRUCT | SOURCE / REFERENCE |
|---|---|---|---|
| p413-$P_{GPD}$ | | *Amp*, *HIS3*, *CEN6*, GPD promoter carrying plasmid | (1) |
| p416-$P_{GPD}$ | | *Amp*, *URA3*, *CEN6*, GPD promoter carrying plasmid | (1) |
| p413-$P_{TEF}$ | | *Amp, HIS3, CEN6,* TEF promoter carrying plasmid | (1) |
| p415-$P_{ADH}$ | | *Amp, LUE2, CEN6*, ADH promoter carrying plasmid | (1) |
| pMT3-hRft1$^{R67C}$-3xFLAG | AP63 | Mammalian expressing plasmid to express hRFT1$^{R67C}$ with C-terminal 3xFLAG tag | Lab stock |
| pMT3-hRft1-3xFLAG | AP65 | Mammalian expressing plasmid to express hRFT1 with C-terminal 3xFLAG tag | Lab stock |
| hRft1-3xFLAG | EcAKM135 | p413-$P_{GPD}$, hRft1-3xFLAG | This study |
| mNG-hRft1-3xFLAG | EcAKM136 | p413-$P_{GPD}$, mNeonGreen-hRft1-3xFLAG | This study |
| hRft1$^{Q21L}$-3xFLAG | EcAKM137 | p413-$P_{GPD}$, hRft1$^{Q21L}$-3xFLAG | This study |
| hRft1$^{R25W}$-3xFLAG | EcAKM138 | p413-$P_{GPD}$, hRft1$^{R25W}$-3xFLAG | This study |
| hRft1$^{R37A}$-3xFLAG | EcAKM139 | p413-$P_{GPD}$, hRft1$^{R37A}$-3xFLAG | This study |
| hRft1$^{R63A}$-3xFLAG | EcAKM140 | p413-$P_{GPD}$, hRft1$^{R63A}$-3xFLAG | This study |
| hRft1$^{R67C}$-3xFLAG | EcAKM141 | p413-$P_{GPD}$, hRft1$^{R67C}$-3xFLAG | This study |
| hRft1$^{A155E}$-3xFLAG | EcAKM142 | p413-$P_{GPD}$, hRft1$^{A155E}$-3xFLAG | This study |
| hRft1$^{A155K}$-3xFLAG | EcAKM143 | p413-$P_{GPD}$, hRft1$^{A155K}$-3xFLAG | This study |
| hRft1$^{E260A}$-3xFLAG | EcAKM144 | p413-$P_{GPD}$, hRft1$^{E260A}$-3xFLAG | This study |
| hRft1$^{R290A}$-3xFLAG | EcAKM145 | p413-$P_{GPD}$, hRft1$^{R290A}$-3xFLAG | This study |
| hRft1$^{R442A}$-3xFLAG | EcAKM146 | p413-$P_{GPD}$, hRft1$^{R442A}$-3xFLAG | This study |
| $P_{GPD}$-ALFA-mNG-hRft1-3xFLAG | EcAKM147 | p413-$P_{GPD}$, ALFA-mNeonGreen-hRft1 | This study |
| $P_{TEF}$-ALFA-mNG-hRft1-3xFLAG | EcAKM148 | p413-$P_{TEF}$, ALFA-mNeonGreen-hRft1 | This study |
| $P_{ADH}$-ALFA-mNG-hRft1-3xFLAG | EcAKM149 | p413-$P_{ADH}$, ALFA-mNeonGreen-hRft1 | This study |
| pCfB2195 | | *Amp, hphMX*, Integration plasmid | Gift from Hiroki Okada (University of Pennsylvania)(2) |
| pCfB2195-$P_{GPD}$-ALFA-mNG-hRft1-3xFLAG | EcAKM150 | pCfB2195, $P_{GPD}$-ALFA-mNeonGreen-hRft1-3xFLAG<br>Plasmids for transformation into yeast chromosomes | This study |
| pCfB2195-$P_{TEF}$-ALFA-mNG-hRft1-3xFLAG | EcAKM151 | pCfB2195, $P_{TEF}$-ALFA-mNeonGreen-hRft1-3xFLAG<br>Plasmids for transformation into yeast chromosomes | This study |

| | | | |
|---|---|---|---|
| pCfB2195-$P_{ADH}$-ALFA-mNG-hRft1-3xFLAG | EcAKM152 | pCfB2195, $P_{ADH}$-ALFA-mNeonGreen-hRft1-3xFLAG<br>Plasmids for transformation into yeast chromosomes | This study |
| pRG205MX | | *Amp, LEU2MX,* Integration plasmid | Gift from Hiroki Okada (University of Pennsylvania)(3) |
| pRG205MX-mCherry-HDEL | EcAKM153 | pRG205MX, mCherry-HDEL$^{\Delta AscI}$<br>Plasmids for transformation into yeast chromosomes | This study |
| pRG205MX-$P_{ADH}$-Nvj1$^{1-121}$-ALFA-nB | EcAKM154 | pRG205MX, $P_{ADH}$-Nvj1$^{1-121}$-ALFA-nB Plasmids for transformation into yeast chromosomes | This study |
| pRS305-mCherry-HDEL | pJF132 | pRS305, mCherry-HDEL Plasmids for transformation into yeast chromosomes | Gift from Jonathan Friedman (University of Texas Southwestern Medical Center) |
| pRS405-$P_{ADH}$-Nvj1$^{1-121}$-ALFA-nB | FFP386 | pRS405, $P_{ADH}$-Nvj1$^{1-121}$-ALFA-nB Plasmids for transformation into yeast chromosomes | Gift from Florian Frohlich (Osnabrück University)(4) |
| pFA6a-2xmNeonGreen-kanMX | | Plasmid for C-terminal integration of 2xmNeonGreen | Gift from Kuninori Suzuki (University of Tokyo)(5) |
| mNG-Alg2 | EcAKM162 | p416-$P_{GPD}$, mNeonGreen-Alg2 | This study |
| mNG-Alg14 | EcAKM163 | p416-$P_{GPD}$, mNeonGreen-Alg14 | This study |
| pCfB2195-$P_{GPD}$-ALFA-mNG-hRft1$^{R37A}$-3xFLAG | EcAKM164 | pCfB2195, $P_{GPD}$-ALFA-mNeonGreen-hRft1$^{R37A}$-3xFLAG<br>Plasmids for transformation into yeast chromosomes | This study |
| pCfB2195-$P_{GPD}$-ALFA-mNG-hRft1$^{R63A}$-3xFLAG | EcAKM165 | pCfB2195, $P_{GPD}$-ALFA-mNeonGreen-hRft1$^{R63A}$-3xFLAG<br>Plasmids for transformation into yeast chromosomes | This study |
| pCfB2195-$P_{GPD}$-ALFA-mNG-hRft1$^{R67C}$-3xFLAG | EcAKM166 | pCfB2195, $P_{GPD}$-ALFA-mNeonGreen-hRft1$^{R67C}$-3xFLAG<br>Plasmids for transformation into yeast chromosomes | This study |
| pCfB2195-$P_{GPD}$-ALFA-mNG-hRft1$^{E260A}$-3xFLAG | EcAKM167 | pCfB2195, $P_{GPD}$-ALFA-mNeonGreen-hRft1$^{E260A}$-3xFLAG<br>Plasmids for transformation into yeast chromosomes | This study |
| pGB1805-Alg2 | | pGB1805, $P_{GAL1}$-Alg2-6xHis-HA-3C protease site-Protein A (ZZ domain) | Horizon Discovery |
| pGB1805-Alg14 | | pGB1805, $P_{GAL1}$-Alg14-6xHis-HA-3C protease site-Protein A (ZZ domain) | Horizon Discovery |
| p416-$P_{GPD}$-mNG-hRft1-3xFLAG | EcAKM170 | p416-$P_{GPD}$, mNeonGreen-hRft1-3xFLAG | This study |

REFERENCES (Table 1)


1. Mumberg, D., Müller, R., and Funk, M. (1995) Yeast vectors for the controlled expression of heterologous proteins in different genetic backgrounds Gene 156, 119-122 10.1016/0378-1119(95)00037-7
2. Stovicek, V., Borja, G. M., Forster, J., and Borodina, I. (2015) EasyClone 2.0: expanded toolkit of integrative vectors for stable gene expression in industrial Saccharomyces cerevisiae strains J Ind Microbiol Biotechnol 42, 1519-1531 10.1007/s10295-015-1684-8
3. Gnugge, R., Liphardt, T., and Rudolf, F. (2016) A shuttle vector series for precise genetic engineering of Saccharomyces cerevisiae Yeast 33, 83-98 10.1002/yea.3144
4. Esch, B. M., Walter, S., Schmidt, O., and Frohlich, F. (2023) Identification of distinct active pools of yeast serine palmitoyltransferase in sub-compartments of the ER J Cell Sci 136, 10.1242/jcs.261353
5. Hirata, E., Ohya, Y., and Suzuki, K. (2017) Atg4 plays an important role in efficient expansion of autophagic isolation membranes by cleaving lipidated Atg8 in Saccharomyces cerevisiae PLoS One 12, e0181047 10.1371/journal.pone.0181047

Table 2. Yeast strains

| YEAST STRAIN NAME | SYSTEMATIC NAME | GENOTYPE | SOURCE / REFERENCE |
|---|---|---|---|
| Wild-type | BY4741 | *MATa his3Δ1 leu2Δ0 met15Δ0 ura3Δ0* | (1) |
| Wild-type | S288C | *MATα SUC2 gal2 mal2 mel flo1 flo8-1 hap1 ho bio1 bio6* | Gift from Maya Schuldiner (Weizmann Institute of Science)(2) |
| *rft1::KANMX4 / RFT1* | YAKM158 | BY4743, *his3Δ1 leu2Δ0 ura3Δ0 rft1::KANMX4 / RFT1* | Yeast Knockout (YKO) Collection (3) |
| KSY512 | KSY512 / YAKM188 | BY4741, *rft1::KANMX4* carrying p416-$P_{GPD}$-*hRFT1*-3xFLAG | This study |
| mCherry-HDEL | YAKM223 | S288C, *mCherry-HDEL-LEU2MX* | This study |
| $P_{GPD}$-mNG-hRft1 mCherry-HDEL | YAKM225 | YAKM223, $P_{GPD}$-*ALFA-mNeonGreen-hRFT1-3xFLAG-hphMX* | This study |
| $P_{TEF}$-mNG-hRft1 mCherry-HDEL | YAKM224 | YAKM223, $P_{TEF}$-*ALFA-mNeonGreen-hRFT1-3xFLAG-hphMX* | This study |
| $P_{ADH}$-mNG-hRft1 mCherry-HDEL | YAKM234 | YAKM223, $P_{ADH}$-*ALFA-mNeonGreen-hRFT1-3xFLAG-hphMX* | This study |
| Erg6-mCherry | ATY502 | BY4741, *ERG6-mCherry::HIS* | Gift from Alexandre Toulmay (University of Texas Southwestern Medical Center) |
| $P_{tet}$-HO | YAKM183 | *URA::CMV-tTA, his3-1 leu2-0 met15-0 HO::kanR-TetO*$_7$*-CYC1*$_{TATA}$*-HO* | Gift from Maya Schuldiner (Weizmann Institute of Science)(4) |
| $P_{tet}$-Rft1 | YAKM147 | *URA::CMV-tTA, his3-1 leu2-0 met15-0 RFT1::kanR-TetO*$_7$*-CYC1*$_{TATA}$*-RFT1* | Gift from Maya Schuldiner (Weizmann Institute of Science)(4) |
| $P_{tet}$-Rft1 $P_{ADH}$-AFLA-mNG-hRft1 | YAKM163 | YAKM147, $P_{ADH}$-*ALFA-mNeonGreen-hRFT1-3xFLAG-hphMX* | This study |
| $P_{tet}$-Rft1 Nvj1-nB $P_{ADH}$-AFLA-mNG-hRft1 | YAKM164 | YAKM163, $P_{ADH}$-*NVJ1*$^{1-121}$*-ALFA-nB-LEU2MX* | This study |
| $P_{GPD}$-mNG-hRft1 Erg6-mCherry | YAKM237 | ATY502, $P_{GPD}$-*ALFA-mNeonGreen-hRFT1-3xFLAG-hphMX* | This study |
| $P_{ADH}$-mNG-hRft1 Erg6-mCherry | YAKM235 | ATY502, $P_{ADH}$-*ALFA-mNeonGreen-hRFT1-3xFLAG-hphMX* | This study |

| | | | |
|---|---|---|---|
| $P_{GPD}$-mNG-hRft1$^{R37A}$ mCherry-HDEL | YAKM248 | YAKM223, *$P_{GPD}$-ALFA-mNeonGreen-hRFT1$^{R37A}$-3xFLAG-hphMX* | This study |
| $P_{GPD}$-mNG-hRft1$^{R63A}$ mCherry-HDEL | YAKM249 | YAKM223, *$P_{GPD}$-ALFA-mNeonGreen-hRFT1$^{R63A}$-3xFLAG-hphMX* | This study |
| $P_{GPD}$-mNG-hRft1$^{R67C}$ mCherry-HDEL | YAKM250 | YAKM223, *$P_{GPD}$-ALFA-mNeonGreen-hRFT1$^{R67C}$-3xFLAG-hphMX* | This study |
| $P_{GPD}$-mNG-hRft1$^{E260A}$ mCherry-HDEL | YAKM251 | YAKM223, *$P_{GPD}$-ALFA-mNeonGreen-hRFT1$^{E260A}$-3xFLAG-hphMX* | This study |

REFERENCES (Table 2)


1. Brachmann, C. B., Davies, A., Cost, G. J., Caputo, E., Li, J., Hieter, P. et al. (1998) Designer deletion strains derived from Saccharomyces cerevisiae S288C: a useful set of strains and plasmids for PCR-mediated gene disruption and other applications Yeast 14, 115-132 10.1002/(SICI)1097-0061(19980130)14:2<115::AID-YEA204>3.0.CO;2-2
2. Mortimer, R. K., and Johnston, J. R. (1986) Genealogy of principal strains of the yeast genetic stock center Genetics 113, 35-43 10.1093/genetics/113.1.35
3. Wach, A., Brachat, A., Pohlmann, R., and Philippsen, P. (1994) New heterologous modules for classical or PCR-based gene disruptions in Saccharomyces cerevisiae Yeast 10, 1793-1808 10.1002/yea.320101310
4. Mnaimneh, S., Davierwala, A. P., Haynes, J., Moffat, J., Peng, W. T., Zhang, W. et al. (2004) Exploration of essential gene functions via titratable promoter alleles Cell 118, 31-44 10.1016/j.cell.2004.06.013

Table 3. Known mutations in Rft1 associated with CDG 1N

| MUTATION | REFERENCE | MODEL OF hRft1 SHOWING MUTATIONS[1] |
|---|---|---|
| R25W | (1) | 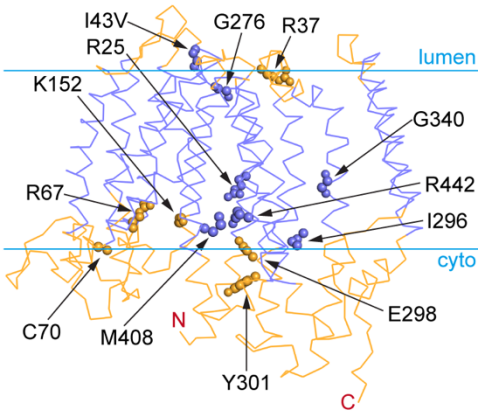  |
| R37L/R442Q | (2) | |
| I43V | (3) | |
| R67C | (4, 5) | |
| C70R | (1) | |
| K152E | (2, 5-7) | |
| G276D | (1) | |
| I296K/I296R | (6) | |
| E298K | (5) | |
| Y301C | (8) | |
| G340S | (9) | |
| R442Q/M408V | (10) | |

[1]AlphaFold model of hRft1, visualized in PyMOL, showing membrane-embedded portions in slate and sections outside the membrane in brightorange. The membrane-embedded portions were estimated from the DeepTMHMM prediction. Residues that are mutated in CDG1N are shown in space-fill. The N-terminus and C-terminus are indicated. Horizontal lines indicate membrane boundaries.

REFERENCES (Table 3)


1. Quelhas, D., Jaeken, J., Fortuna, A., Azevedo, L., Bandeira, A., Matthijs, G. et al. (2019) RFT1-CDG: Absence of Epilepsy and Deafness in Two Patients with Novel Pathogenic Variants JIMD Rep 43, 111-116 10.1007/8904_2018_112
2. Aeby, A., Prigogine, C., Vilain, C., Malfilatre, G., Jaeken, J., Lederer, D. et al. (2016) RFT1-congenital disorder of glycosylation (CDG) syndrome: a cause of early-onset severe epilepsy Epileptic Disord 18, 92-96 10.1684/epd.2016.0802
3. Papi, A., Zamani, M., Shariati, G., Sedaghat, A., Seifi, T., Negahdari, S. et al. (2023) Whole exome sequencing reveals several novel variants in congenital disorders of glycosylation and glycogen storage diseases in seven patients from Iran Mol Genet Genomic Med 11, e2099 10.1002/mgg3.2099
4. Haeuptle, M. A., Pujol, F. M., Neupert, C., Winchester, B., Kastaniotis, A. J., Aebi, M. et al. (2008) Human RFT1 deficiency leads to a disorder of N-linked glycosylation Am J Hum Genet 82, 600-606 10.1016/j.ajhg.2007.12.021
5. Vleugels, W., Haeuptle, M. A., Ng, B. G., Michalski, J. C., Battini, R., Dionisi-Vici, C. et al. (2009) RFT1 deficiency in three novel CDG patients Hum Mutat 30, 1428-1434 10.1002/humu.21085
6. Jaeken, J., Vleugels, W., Regal, L., Corchia, C., Goemans, N., Haeuptle, M. A. et al. (2009) RFT1-CDG: deafness as a novel feature of congenital disorders of glycosylation J Inherit Metab Dis 32 Suppl 1, S335-338 10.1007/s10545-009-1297-3
7. Barba, C., Darra, F., Cusmai, R., Procopio, E., Dionisi Vici, C., Keldermans, L. et al. (2016) Congenital disorders of glycosylation presenting as epileptic encephalopathy with migrating partial seizures in infancy Dev Med Child Neurol 58, 1085-1091 10.1111/dmcn.13141
8. Bastaki, F., Bizzari, S., Hamici, S., Nair, P., Mohamed, M., Saif, F. et al. (2018) Single-center experience of N-linked Congenital Disorders of Glycosylation with a Summary of Molecularly Characterized Cases in Arabs Ann Hum Genet 82, 35-47 10.1111/ahg.12220
9. Abiramalatha, T., Arunachal, G., Muthusamy, K., and Thomas, N. (2019) A family with floppy neonates with severe respiratory insufficiency: A lethal phenotype of RFT1-CDG due to a novel mutation Eur J Med Genet 62, 248-253 10.1016/j.ejmg.2018.07.023
10. Ondruskova, N., Vesela, K., Hansikova, H., Magner, M., Zeman, J., and Honzik, T. (2012) RFT1-CDG in adult siblings with novel mutations Mol Genet Metab 107, 760-762 10.1016/j.ymgme.2012.10.002